Assessing the quality of models of the ambient solar wind

Article

Published Version

Key Points:
- Presents a review of the history, current status, and prospects for models of the ambient solar wind
- The review covers model quality from the perspective of both operational forecasting and scientific research support
- The review anticipates model and data input improvements expected over the next decade

Correspondence to:
P. MacNeice,
Peter.J.MacNeice@nasa.gov

Assessing the Quality of Models of the Ambient Solar Wind

P. MacNeice[1] ![ID], L. K. Jian[1] ![ID], S. K. Antiochos[1], C. N. Arge[1], C. D. Bussy-Virat[2] ![ID], M. L. DeRosa[3] ![ID], B. V. Jackson[4] ![ID], J. A. Linker[5], Z. Mikic[5], M. J. Owens[6] ![ID], A. J. Ridley[2], P. Riley[5] ![ID], N. Savani[1,7] ![ID], and I. Sokolov[2]

[1]Heliophysics Science Division, NASA Goddard Space Flight Center, Greenbelt, MD, USA, [2]Department of Climate and Space Sciences and Engineering, University of Michigan, Ann Arbor, MI, USA, [3]Lockheed Martin Solar and Astrophysics Laboratory, Palo Alto, CA, USA, [4]Center for Astrophysics and Space Sciences, University of California, San Diego, La Jolla, CA, USA, [5]Predictive Science Inc., San Diego, CA, USA, [6]Department of Meteorology, University of Reading, Reading, UK, [7]GPHI, University of Maryland, Baltimore County, MD, USA

Abstract In this paper we present an assessment of the status of models of the global solar wind in the inner heliosphere. We limit our discussion to the class of models designed to provide solar wind forecasts, excluding those designed for the purpose of testing physical processes in idealized configurations. In addition, we limit our discussion to modeling of the *ambient* wind in the absence of coronal mass ejections. In this assessment we cover use of the models both in forecast mode and as tools for scientific research. We present a brief history of the development of these models, discussing the range of physical approximations in use. We discuss the limitations of the data inputs available to these models and its impact on their quality. We also discuss current model development trends.

1. Introduction

This paper presents an assessment of the status of models of the solar wind in the inner heliosphere. It is intended to assess progress resulting from the community-wide efforts to create a robust solar wind forecasting capability that can be used in an operational setting. We also identify prospects for future model improvements.

We focus on models that are designed toward a future in forecasting the state of the global inner heliospheric solar wind. We exclude those designed for the purpose of testing physical processes in idealized configurations, although we anticipate how they may impact future developments of the forecast models. In addition, we limit our discussion to modeling of the *ambient* wind in the absence of coronal mass ejections.

Our assessment is split into six sections. The first, section 2, presents a brief history of the development of relevant models from their origin up to the present. Section 3 presents a summary of the current capabilities of the models from both the operational and research user perspective. In section 4 we discuss issues associated with the model inputs and how these are being addressed. Section 5 discusses some physical processes that are still not incorporated into the models, and finally, section 6 offers our conclusions.

This paper is designed to illustrate the development history and status of the models, not to be a comprehensive review of the complete literature in the field. In the interest of brevity, the narrative of model history is developed by selecting a few models whose stories serves to illustrate the common development of their model classes.

2. Model History

In this section we briefly review the history of the development of models of the ambient corona and solar wind. In organizing this, we proceed from models with the simplest physical approximations, which rely most heavily on empirical tuning, to the most sophisticated. The models we reference are listed in Table 1. Those models without an explicit name are listed under the model developer's name(s).

2.1. Empirical Models

Modeling of the solar coronal magnetic field began in earnest in the early 1960s with the advent of computers and the availability of photospheric magnetograms. The earliest models of the inner coronal field were based

Table 1
Models Referenced in This Paper

Model name	Type	Spatial domain
PDF	Empirical pattern matching	L1
PROJECTZED	Empirical pattern matching	L1
AnEn	Empirical pattern matching	L1
PFSS	Potential field	Corona
NLFFF	Force-free field	Corona
Yeates et al.	3-D magnetofriction	Corona
WSA	Potential + semiempirical kinematic	Corona + inner heliosphere
HAF	Potential + semiempirical kinematic	Corona + inner heliosphere
ESWF	Empirical from coronal hole EUV	L1
WSA/ENLIL	Potential + 3-D MHD	Corona + inner heliosphere
HHMS	Potential + 3-D MHD	Corona + inner heliosphere
Usmanov	Potential + 3-D MHD	Corona + inner heliosphere
SIP-CESE	Potential + 3-D MHD	Corona + inner heliosphere
LFM_Helio (now GAMERA)	Potential + 3-D MHD	corona + inner heliosphere
CRONOS	Potential + 3-D MHD	Corona + inner heliosphere
EUHFORIA	Potential + 3-D MHD	Corona + inner heliosphere
SUSANOO-SW	Potential + 3-D MHD	Corona + inner heliosphere
MS-FLUKSS	Potential + 3-D MHD	Corona + inner heliosphere
REPPU	3-D MHD	Corona + inner heliosphere
Hayashi	3-D MHD	Corona + inner heliosphere
CORHEL	Model suite (potential and MAS 3-D MHD)	Corona + inner heliosphere
AWSoM_R	Part of SWMF (potential and 3-D MHD)	Corona + inner heliosphere
CGEM	Model suite (3-D magnetofriction + MHD)	Corona + inner heliosphere
HelTomo	3-D tomographic	Inner heliosphere
ADAPT	Flux evolution	Solar surface
SURF	Flux evolution	Solar surface
AFT	Flux evolution	Solar surface
ESFTM	Flux evolution	Solar surface

Note. PFSS = potential field source surface; WSA = Wang-Sheeley-Arge; HAF = Hakamada-Akasofu-Fry; ADAPT = Air Force Data Assimilative Photospheric Flux Transport; ESWF = Empirical Solar Wind Forecast; PDF = probability distribution function; AnEn = Analogue Ensemble; HelTomo = heliospheric 3-D reconstruction inversion tomography; EUHFORIA = EURopean Heliospheric FORecasting Information Asset; REPPU = REProduce Plasma Universe; CGEM = Coronal Global Evolutionary Model; EUV = extreme ultraviolet; MHD = magnetohydrodynamic; SWMF = Space Weather Modeling Framework; MAS = MHD about a Sphere; NLFFF = Non-Linear Force Free Field; SIP-CESE = Solar-InterPlanetary space-time Conservation Element and Solution Element; LFM_Helio = Lyon-Fedder-Mobarry Heliospheric; MS-FLUKSS = Multi-Scale Flux Kinetic Simulation Suite; CORHEL = CORonal and HELisopheric Model Suite; AWSoM-R = Alfven Wave Solar Atmospheric Model; SURF = SURface Flux Transport; AFT = Advective Flux Transport; ESFTM = Evolving Surface Flux Transport.

on current free potential solutions. The potential field source surface (PFSS) approach was developed in the late 1960s (Altschuler & Newkirk, 1969; Schatten et al., 1969) using spherical harmonic expansion (Chapman & Bartels, 1940; Gauss, 1839) of the solution and extended to include a current sheet by Schatten (1971). This work provided the coronal model foundation for the Wang-Sheeley (WS) model. Based on observed inverse correlations between the wind speed and the coronal field expansion factor (Sheeley & Wang, 1991; Wang & Sheeley, 1990), an empirical model of the solar wind speed was developed. With subsequent improvements, including a revised empirical formula, which also takes account of the proximity of field line foot points to the nearest coronal hole boundary, the model became the Wang-Sheeley-Arge (WSA) model (Arge & Pizzo, 2000). Recently, Riley et al. (2015) have pointed out that the distance from the coronal hole boundary seems to be more important for accurate models than the expansion factor.

The WSA model uses a spherical source surface, which is almost always located at $2.5R_\odot$, where $R_\odot$ is the solar radius. A number of authors (Levine et al., 1982; Schulz et al., 1978) have explored the effects of nonspherical source-surface shapes, and Zhao and Hoeksema (1994) provided a current sheet source surface model, which includes the effect of a current outside the PFSS domain. Although most modeling efforts use the PFSS model, and it remains the only one in active operational use (Luhmann et al., 2002), there is one notable exception of its use in passive forecasts of field in the heliospheric 3-D reconstruction inversion tomography (HelTomo) interplanetary scintillation (IPS)-based heliographic tomography model (Dunn et al., 2005; Jackson et al., 2016).

WSA has become one of the workhorse models of the research and forecasting communities.

Current operational versions of WSA at both National Oceanic and Atmospheric Administration's Space Weather Prediction Center and the Community Coordinated Modeling Center (CCMC) use single synoptic photospheric magnetograms for input. The next version, to be released shortly, will also be able to process time-evolving series of synoptic maps produced by the Air Force Data Assimilative Photospheric Flux Transport (ADAPT) project (see section 4).

The Hakamada-Akasofu-Fry model (Fry et al., 2001) is similar in general design to the WSA model and, as reported by Norquist and Meeks (2010), achieves similar performance for both wind speed and interplanetary magnetic field (IMF) polarity predictions.

The Empirical Solar Wind Forecast (ESWF) model (Empirical Solar Wind Forecast, 2018; Reiss et al., 2016), is based on an empirical relation between the areas of coronal holes as observed in extreme ultraviolet (EUV) and the solar wind speed forecast at L1 4 days after the coronal hole observations. The ESWF operational tool, which is currently running at the University of Graz (Empirical Solar Wind Forecast, 2018), uses hourly updated images from the Atmospheric Imaging Assembly (AIA) on board the Solar Dynamics Observatory (SDO), and an automated coronal hole detection algorithm.

The WSA, Hakamada-Akasofu-Fry, and ESWF models apply extensive empirical tuning in order to achieve their forecast quality. In contrast, models such as the probability distribution function (PDF) model (Bussy-Virat & Ridley, 2014), PROJECTZED (Riley et al., 2017), and the Analogue Ensemble (AnEn) model (Owens et al., 2017) are purely empirical.

The PDF model forecasts the wind speed at L1 up to 5 days in advance using probability distributions, which have been constructed by analyzing solar wind observations between 1995 and 2011. These PDFs specify the likelihood that a particular wind speed will occur, given the current speed and the current slope of the wind speed curve. The model also takes account of rotational periodicities at quiet times and was updated (Bussy-Virat & Ridley, 2016) to improve its ability to identify stream interaction regions (SIRs). The PDF model has recently been installed at the CCMC.

PDF is just one of a range of possible probabilistic forecasting approaches. Owens et al. (2017) provide some initial results using an approach borrowed from the atmospheric weather forecasting community, called the AnEn, or *similar day* approach. In this method, and in a similar model called PROJECTZED (Riley et al., 2017), intervals from the past, which *resemble* the most recent time window, are used in ensemble fashion to predict what the wind will look like in the immediate future. Based on their initial evaluation, this approach, as configured in their tests, appears to outperform persistence. Owens et al. (2017) conclude that "the AnEn approach is very promising for short or medium lead-time solar wind and geomagnetic forecasting (hours to days) and thus may serve as a complementary approach to the longer lead-time (days to weeks) physics-based magnetohydrodynamic models." However, their exploration of how best to tune this approach is still in its infancy, and improved performance can be anticipated.

2.2. Force-Free Models of the Coronal Field
Potential field models of the corona make the simplifying assumption that the corona has no electrical current. This is not true but does allow for analytic solutions that match the photospheric field measurements and which can be computed quickly, which is why models based on the potential field approximation, such as WSA, have been and remain so popular.

To properly model currents in the corona requires full magnetohydrodynamic (MHD) modeling. Because MHD models are computationally more intensive and the full complement of boundary conditions (which include

photospheric density and temperature information) are typically not available, their algorithmic complexity makes them less robust than simpler models.

A popular compromise approach has been to allow for currents in the corona, but to insist that these are always aligned with the local magnetic field. This means that the Lorentz force, which the magnetic field exerts on the plasma, given by $\mathbf{J} \times \mathbf{B}$, is zero, which is why this class of models is called *Force Free*.

To justify this approach, it is argued that the magnetic field dominates the plasma in the corona. This is not true in the photosphere or in the heliosphere. Gary (2001) presented a one-dimensional model for the magnetic stratification of the solar atmosphere using observations at different heights and argued that there is a range of heights in the solar atmosphere, between the chromosphere and about 100 Mm, where the plasma β, the ratio of plasma pressure to magnetic pressure, is $\ll 1$. Within this height range, the magnetic pressure is so much larger than gas pressure that neither gas pressure gradients nor the gravitational force can effectively balance any Lorentz forces, which might develop, and therefore, if the field is in an equilibrium configuration, it must be approximately force free.

Aly (1989) and Amari et al. (1997) introduced many of the constraints to which practical force-free models, based on observation, should adhere. Since then a number of different algorithms have been applied or developed (see the reviews in; Wiegelmann, 2008; Wiegelmann & Sakurai, 2012). A number of papers were published in the early 2000s testing these algorithms on analytically constructed test solutions (DeRosa et al., 2009, 2015; Metcalf et al., 2008; Schrijver et al., 2008, 2006). These codes require vector magnetogram data. However, prior to the HINODE and SDO missions, very little usable vector magnetogram data existed. Regnier and Fleck (2004) and Wiegelmann et al. (2005) published the first force-free models based on actual observations for limited size fields of view containing a few targeted active regions.

Nonlinear force-free models were originally developed to understand the buildup of free energy in active regions. More recently, these models have been extended from cartesian to spherical geometry and applied to large field-of-view data and even to the global coronal field (Tadesse et al., 2014).

Yang et al. (1986) pointed out that the time-independent nonlinear force-free field problem can be solved by using a time-dependent MHD code in which the plasma velocity has been replaced with a frictional force that is proportional to the Lorentz force. This is called the *magnetofrictional model*. The standard nonlinear force-free field solution is achieved if the system is allowed to reach an equilibrium.

Since then, Mackay and van Ballegooijen (2006) and Yeates et al. (2008) have coupled a global magnetofrictional code to a surface flux transport model (Yeates et al., 2007) to create a time-dependent quasi-static evolution of the coronal field. This follows the evolution of the coronal magnetic field through a sequence of nonlinear force-free fields in response to the observed photospheric field evolution and flux emergence. The model aims to follow the long-term continuous buildup of free magnetic energy and electric currents in the corona.

To date no force-free models are in use for operational forecasting. The Non-Linear Force Free Field (NLFFF) code (Tadesse, 2015; Wiegelmann, 2007) is installed and in use at the CCMC and is part of the SDO product pipeline.

In anticipation of their application to SDO Helioseismic and Magnetic Imager (HMI) photospheric vector magnetogram data, the performance of many of these codes was analyzed. Schrijver et al. (2006) considered their performance when applied to synthetic data with known solutions and guaranteed force-free conditions at the lower boundary and found them to be reliable and accurate. Applying these techniques to more realistic modeling data (Metcalf et al., 2008) and to real vector magnetograms from Hinode SOT-SP (DeRosa et al., 2009) indicated several issues with the NLFFF paradigm.

They concluded that four conditions were likely to improve the chances for successful application of NLFFF models. These were

- that they cover large volumes at high resolution to minimize the influence of side boundaries,
- that they accommodate measurement uncertainties (in particular in the transverse field component) in the formulation of the lower boundary condition,
- that they preprocess the lower-boundary vector field to achieve near-force-free field as would be found in the high chromosphere, and

- that they assimilate coronal observations to constrain the solutions, such as discussed in Malanushenko et al. (2012) and Malanushenko et al. (2014).

Additionally, the use of higher-resolution boundary data are shown to benefit estimates of free energy and magnetic helicity within the NLFFF solutions (DeRosa et al., 2015). As discussed above, some of these code improvements have already been developed and SDO now provides a large data set of full disk vector magnetogram data.

Recently, Peter et al. (2015) challenged the use of these codes for the purposes of estimating the magnetic free energy in active regions. They analyzed the order of error in the approximation to be equal to the value of β and confirmed this by comparing their results with the equivalent solutions from an MHD code. They found the error in total energy to be of the same order as the estimated total free energy. This suggests that to be useful in supporting models of the ambient solar wind, force-free models should be supported by imaging analysis of active region loops, as suggested by Peter et al. (2015) and tested by Chifu et al. (2017; see also; Warren et al., 2018), or should be extended to include both gas pressure gradients and gravity as in magnetohydrostatic equilibrium models (Zhu & Wiegelmann, 2018).

2.3. Tomographic Solar Wind Reconstruction Models

For a general review of the development of tomographic techniques for the reconstruction of the solar wind state we refer to Jackson et al. (2011).

The state of the art in this area is the University of California, San Diego (UCSD) IPS HelTomo code. Originally developed by Jackson et al. (1998), and modified into a time-dependent code in later versions (Jackson et al., 2002), HelTomo is based on matching observed scintillations of astronomical radio sources that are viewed through the intervening solar wind plasma. Because the solar wind plasma contains both the ambient wind and occasionally CMEs, CMEs are imbedded in the observations and cannot easily be separated from the ambient. HelTomo sets up a trial solar wind state at a *source surface* or inner boundary, typically set to be 15 solar radii. The wind state at the source surface is then propagated outward, using a simple kinematic approximation, to define a 3-D heliospheric model of density and/or velocity. This reconstruction is then used to compute the scintillations expected from the set of astronomical radio sources. The predicted scintillations are compared with actual observations along each radio source line of sight (LOS). Differences between the predicted and observed scintillation patterns are then used, in an iterative process to update the solar wind state at the inner boundary, until a good match is achieved between observation and forecast. This original HelTomo algorithm has since been extended to incorporate in situ wind speed (Jackson et al., 2010) and density (Jackson et al., 2013) measurements as constraints in the tomographic reconstruction. The UCSD group maintains a website where they post nowcasts and forecasts of the state of the solar wind (http://ips.ucsd.edu/high_resolution_predictions).

For many years the model has been based on scintillation data from the Institute for Space-Earth Environmental research STELab radio array in Japan. The HelTomo team are in the process of extending their data sources to include data sets from other observatories around the globe, including from the Ooty array, the Big Scanning Array in Russia, the Mexican Radio Array Telescope, the Murchison Widefield Array in Western Australia, and the Low Frequency Array based in the Netherlands. Inclusion of observations from other observatories can provide potentially much larger data sets that the Institute for Space-Earth Environmental research IPS system can alone provide, and in addition will benefit from more continuous coverage of the solar wind condition near the Sun.

They have also been experimenting with use of more sophisticated wind propagation methods, such as the ENLIL MHD code, both as an upgrade to the HelTomo model and as a method to initialize the MHD models of the solar wind with a more accurate starting state (Jackson et al., 2015; Yu et al., 2015). This IPS-driven ENLIL system is run in real time at both George Mason University and the Korean Space Weather Center. The advantage of this system is that it can show and forecast the propagation of both ambient solar wind structures as well as CMEs without human intervention.

HelTomo was one of the first solar wind models presented to the CCMC at the Goddard Space Flight Center circa the year 2000.

2.4. MHD Codes

The first 3-D MHD model of the ambient global corona and heliosphere based on photospheric magnetic field data was that of Usmanov (1993). This model used a PFSS model to initialize the inner coronal field

and set surface boundary conditions. It divided the full simulation into two domains, an outer region of supersonic/super-Alfvénic flow from $r^* = 9.8R_\odot$, and an inner region from the surface to r^*, with different algorithms applied to the two regions.

This approach of coupling different codes beyond the sonic and Alfvénic points has been followed in almost all MHD solar wind models since then. In some cases, the inner region is modeled using WSA, and the outer region using an MHD algorithm (e.g., ENLIL, Odstrcil, 2003; HHMS, Detman et al., 2006; GAMERA, previously known as Lyon-Fedder-Mobarry Heliospheric, Merkin et al., 2011; CRONOS, Wiengarten et al., 2013; EURopean Heliospheric FORecasting Information Asset, Pomoell & Poedts, 2018; SUSANOO-SW, Shiota et al., 2014; and Multi-Scale Flux Kinetic Simulation Suite, Kim et al., 2018). In other cases MHD codes are used for both regions (e.g., CORonal HELiospheric [CORHEL] and Alfvén Wave Solar Atmospheric Model [AWSoM_R], van der Holst et al., 2014; Solar InterPlanetary space-time Conserving Element and Solution Element MHD, Feng et al., 2012; Hayashi, 2012; and REProduce Plasma Universe, Den et al., 2015; Nakamizo et al., 2009).

Over the last 20 years these MHD codes have evolved to improve the physical processes that are included, to improve the underlying algorithms, their user interfaces, and the efficiency with which they execute. The development history of the MHD about a Sphere (MAS) code, which is part of the CORHEL model suite, offers a typical illustration of the discipline's progress.

In 1999, Mikić et al. (1999) used a 3-D MHD code (MAS) with an adiabatic energy equation and a reduced polytropic index to model the global corona out to $30R_\odot$. They used a polytropic equation of state for simplicity, with a reduced value of $\gamma = 1.05$, based on Parker's (1963) observation that the coronal temperature does not vary significantly. Not surprisingly, such a simple energy equation fails to reproduce the fast/slow flow speed contrast, (see also ; Cohen, 2017), and the contrast in temperature and density observed between streamers and coronal holes. These flaws were addressed by improving the energy equation in the model to include parallel thermal conduction along the magnetic field lines, radiative losses, and a coronal heating source. This has been called the *thermodynamic* model.

In 2001 Lionello et al. (2001) demonstrated a 2-D version of the thermodynamic MAS code, and in 2003 Lionello et al. (2003) presented initial 3-D results from the thermodynamic MAS code for the global corona. Riley et al. (2001) published a coupled model of the corona and heliosphere that applied the MAS *polytropic* code separately in the corona and heliosphere but reprocessed the solution at the outer boundary of the coronal component to provide inner boundary flows of the right order for the heliosphere.

In 2011 Riley et al. (2011) modeled the coupled corona/heliosphere with both polytropic and thermodynamic versions and concluded that the *empirically adjusted* polytropic code still outperformed the physically more complete thermodynamic version. More recently, Lionello et al. (2013) introduced turbulent Alfvén wave heating to the model and Lionello, Velli, Downs, Linker, Mikić, and Verdini (2014) validated a time-dependent turbulent Alfvén wave heating model of the solar wind with the thermodynamic code. Linker et al. (2016) have since used ADAPT maps to drive a time-dependent MAS solar wind model coupled to the WSA coronal field model. Approaches have been developed to add embedded flux ropes into the coronal field solutions to allow for the influence of large filament structures on the global field topology (Titov et al., 2018, 2014). As the model has been developed, significant work has also been done in developing diagnostic tools to support comparison of model results with observations (e.g., Downs et al., 2010; Gibson et al., 2016; Winebarger et al., 2014), and to analyze the complex magnetic topologies (Titov, 2007).

While the PredSci (PSI) team was developing the CORHEL model suite and its component codes, other models were following similar development tracks and developing comparable capabilities. The University of Michigan group led by Professor Tomas Gombosi developed the Space Weather Modeling Framework (Tóth et al., 2005) built around their BAT-S-RUS MHD code (Gombosi et al., 2001; Powell et al., 1999). It incorporates a model of the coupled corona and inner heliosphere, supporting a similar range of physical processes (Roussev et al., 2003; Tóth et al., 2005) as CORHEL, and includes Alfvén wave heating in the AWSoM_R model version (Meng et al., 2015; van der Holst et al., 2014). In addition, it can represent multiple species with different gyrotropic temperatures. Wiengarten et al. (2016) have also coupled their CRONOS (Wiengarten et al., 2013) code to equations for the evolution of turbulent Alfvénic fluctuations.

In 2004, Arge and Odstrcil began working to couple WSA with Odstrcil's 3-D MHD model of the heliosphere, which was subsequently named ENLIL. The coupled WSA/ENLIL model has become one the workhorse models of both research and forecast communities (see; Sheeley, 2017). As of April 2018, the CCMC has used

these models to service more than 7,000 user requests for ambient solar wind runs and has executed more that 20,000 near-real-time WSA/ENLIL runs to feed its Integrate Space Weather Analysis system. In 2011 WSA/ENLIL was made operational at the National Oceanic and Atmospheric Administration's Space Weather Prediction Center (Pizzo et al., 2011).

Odstrcil et al. (2004) described a similar coupling of the ENLIL heliospheric model with the MAS coronal model. Merkin et al. (2016) described a coupling of the Lyon-Fedder-Mobarry Heliospheric model with the MAS coronal model.

3. Assessment of Current Model Capabilities

In this section we present a summary of the capabilities of the current generation of models available for either operational forecasting use or for use by users through the services of the CCMC. It should be noted that this review relies on validation and quality assessment studies done in some instances by the model's developer and in others independently by the community or the CCMC.

We begin in section 3.1 by reviewing results on the quality of forecasts at L1 of the empirical models, WSA, PDF, PROJECTZED, and AnEn. These models are inexpensive to run and focus on a limited set of wind parameters. It is easy, therefore, to generate formal metric based assessments for these models covering forecasts of specific parameters for long time intervals, resulting in clear quantitative model scores.

For more computationally expensive MHD codes, the validation literature is much less coherent. It consists of multiple studies using different code combinations, focusing on different features of the wind solution, using different methodologies, and covering different time periods. We summarize this with a review of the literature in section 3.3, and where possible, connect the reported performance levels to the quantitative assessment of the empirical codes.

The MHD codes are capable, when pushed to their limits by their developers, of more sophisticated scientific modeling than is examined in any of the validation studies. We discuss the most important of these capabilities in sections 3.4 to 5.1.

3.1. Assessment of Empirical Near-Real-Time Models

We illustrate the quality of empirical models by concentrating on the WSA, PDF, PROJECTZED, and AnEn models. PDF, PROJECTZED, and AnEn are purely empirical models that can forecast solar wind properties for which there is an extensive observational record at L1.

The PDF model forecasts wind speed up to 5 days in advance. It develops probability distributions that are constructed by analyzing solar wind observations between 1995 and 2011. The probability distributions specify the likelihood that a particular wind speed will occur, given the current speed and the current slope of the wind speed curve. The model also takes account of rotational periodicities at quiet times and was updated (Bussy-Virat & Ridley, 2016) to improve its ability to identify SIRs.

The PROJECTZED model considers a forecast window Δt. It identifies the observations from the most recent Δt interval, then slides that window backwards in time, 1 hr at a time, comparing each window's observations with the most recent. It uses the OMNI database going back to the early 1970s. It saves the 50 windows that best match the most recent window and uses the period Δt following each of these, to produce a forecast ensemble for the upcoming window. The mean of this ensemble is the models forecast. PROJECTZED can forecast wind speed, proton number density and temperature, and components of the magnetic field.

AnEn uses a similar approach but can perform multivariable pattern matching (e.g., forecasting wind speed by simultaneously matching both wind speed and proton number density) and allows the user to vary the number of past intervals included in the ensemble. It can also forecast wind speed, proton number density, and components of the magnetic field.

The essential results, which we detail in section 3.1.1 to 3.1.3, are that for the plasma parameters and for the radial and tangential components of the IMF, for forecast windows of 6 hr or less these models work well. For longer forecast windows they continue to outperform both persistence and climatological (the average observed value over time) before eventually approaching the climatological forecasts for windows of approximately 100 hr and longer. These quantities are typically determined by the larger-scale features of the wind with temporal coherence of hours to days, and so the pattern matching techniques can work effectively.

However, the processes that establish the component of the IMF out of the plane of the ecliptic, B_N (in RTN coordinates), are generally short scale both spatially and temporally. As a result, the pattern matching techniques are poorly suited to forecast it. For B_N, while some models do slightly better that the climatological model ($B_N = 0$) for forecast windows of 6 hr or less, they are typically no better than the climatological forecast for longer times.

3.1.1. Wind Speed Forecasts

Owens et al. (2017) compared the AnEn median model forecast for solar wind speed at L1 to the OMNI hourly data set and computed the root-mean-square error (RMSE). For the period from January 1996 through December 2014, for a 24-hr forecast, the AnEn model achieved an RMSE of 48 km/s. RMSE is not reported by Riley et al. (2017) for PROJECTZED, but its methodology is sufficiently similar to that of AnEn, that we would except a similar result. For the PDF model Bussy-Virat and Ridley (2014) report RMSE for a 24-hr forecast of 83 km/s for the year 2008 and 66 km/s for the year 2011, illustrating how pattern matching model forecast quality can depend on the time period being studied. For reference, the persistence model achieves an average RMSE of approximately 70 to 80 km/s for a 24-hr forecast.

Thus, for the pattern matching models for the 24-hr L1 wind speed forecast, over an extended period, the RMSE is expected to be in the range from 50 to 80 km/s.

For an older version of the WSA model, Owens et al. (2005) report annual RMSE for 24-hr forecast for the years between 1995 and 2002, with model runs made using photospheric synoptic magnetograms from the Mount Wilson Observatory. The yearly averages ranged from 76 to 109 km/s with an average of 93 km/s.

For a short interval from 2011 to 2014, Reiss et al. (2016) found that for 4-day forecasting the ESWF gave an RMSE of 108 km/s, while for that period WSA gave 99 km/s.

As the forecast window increases, the performance of the pattern matching models deteriorates but always beats the persistence model. In contrast, the WSA model performance stays relatively constant, apparently independent of the length of the forecast window. For forecast windows less than 3 days it is outperformed by the pattern matching models, but for longer windows it matches their performance. For windows longer that 3 days all models approach the performance of the *climatological* forecast, which assumes that the wind is always at the average observed wind speed.

We can also judge these models based on their ability to forecast events such as High-Speed Events (HSEs) where the wind quickly transitions from slow to fast speed, and crossings of the heliospheric current sheet (HCS). Bussy-Virat and Ridley (2016) studied PDF and WSA forecasts for HSEs between 1995 and 2012. They report that if a HSE occurred in the next 24 hr, the PDF model made a successful forecast (a *hit*) 20% of the time and *missed* 80% of the time. Thirty-three percent of its forecasted HSEs were false positives. When forecasting no HSE in the next 24 hr the model was correct approximately 90% of the time. When they compared the PDF results with those of WSA, they found similar rates of hits and misses, and for forecasting that no event would occur, but found that WSA had 3 times more false positives. These results clearly depend to some extent on how you define a HSE and what criteria you use to determine hits and misses, but the WSA results that they report are generally consistent with those of MacNeice (2009) and Owens et al. (2005).

The different time windows and methodologies used to analyze both the RMSE and event forecasts highlight a need for a consistent validation.

3.1.2. Wind Density Forecasts

For forecast windows of 2 hr or less, persistence outperforms the AnEn model wind density forecasts, but for all longer forecast time windows AnEn always beat both persistence and climatological. For a forecast window of 24 hr it achieved an RMSE of 2.5 cm^{-3}. For forecasts of 80 hr and beyond the wind density RMSE asymptotes to a value of 3 cm^{-3} compared to the climatological value of 3.5 cm^{-3}.

3.1.3. Magnetic Field Forecasts

Forecasting the IMF and particularly its north-south component is of most interest for interplanetary coronal mass ejections. Occasionally, however, and particularly during the declining and solar cycle minimum phases, corotating interaction regions can introduce a sufficiently strong southward component in the ambient wind to produce geoeffective disturbances (Echer et al., 2017).

Both AnEn and PROJECTZED also forecast the components of the IMF at L1.

AnEn reports results for the components of **B** in RTN coordinates, with B_N representing the out of ecliptic plane component and B_T the component in the plane of the ecliptic. For B_T the relative performance of AnEn

compared to both persistence and recurrence is qualitatively similar to that for wind speed, in that the model outperforms both for all forecast windows but approaches the climatological forecast for time windows of order 100 hr. Persistence beats climatological for forecast windows of less than 15 hr, but for longer windows climatological significantly outperforms persistence.

For B_N, however, which is generally of more significance to forecasters, the pattern is markedly different. Persistence outperforms climatological only for forecast windows of less than 2 hr. This is due to the known short autocorrelation time in the observed B_N time series (e.g., Lockwood et al., 2016) and illustrates the challenge associated with predicting B_N. AnEn outperforms climatological for forecasts of 10 hr or less, beyond which it tracks but is slightly worse than climatological.

Riley et al. (2017) report similar qualitative conclusions for the performance of PROJECTZED in forecasting the components of the IMF, although, as already noted, they do not report RMSE scores over an extended period of time.

3.2. Comparing Near-Real-Time Tomography to Empirical Models

There is a very limited set of published results that we can use to compare the HelTomo model with the empirical models. Jian et al. (2015) included HelTomo in a list of CCMC-hosted models validated for the Carrington Rotations 2056 to 2062, from May to November 2007. They found a wind speed RMSE for HelTomo of 63 km/s for the time interval, easily beating 24-hr persistence, which returned a RMSE of 83 km/s. This suggests that HelTomo ranks between the empirical models and WSA when measured against RMSE forecast. However, there is too little published validation data to claim this as a robust relative ranking.

3.3. Literature Review of MHD Model Validation Studies

Validation studies of the MHD models have been done by the model developers and by users of those models, which are hosted at the CCMC. These studies have explored a range of metrics examining various locations and structures in the solution. A review of this literature supports the following conclusions, based on the model use of static synoptic magnetograms.

In the corona, comparing the MHD solution with pure PFSS models (e.g., Wiegelmann et al., 2017),

- the MHD code coronal solutions typically reproduce the same large-scale structure (i.e., patterns of open and closed flux) as the potential models and the same general location and shape for the neutral line at the base of the HCS streamer base;
- the MHD codes produce more realistic cusp like topologies at the tip of the HCS streamer where the PFSS models produce more rounded structure;
- field lines in the PFSS model are typically shorter than those in their MHD equivalents; and
- PFSS models (using the typical source surface radius value of 2.5 solar radii) appear to underestimate the amount of open flux in the heliosphere.

In the heliosphere, validation work has focussed on operational style metrics (typically at L1, but occasionally for very limited time windows at Mars, Mercury, Venus, and at the location of spacecraft including Ulysses and STEREO A and B), and on the location and arrival times of SIRs and current sheet crossings at L1.

With few exceptions, such as Gressl et al. (2014), the validation studies of MHD solutions for the ambient wind in the heliosphere have used codes driven at their inner boundary by WSA (or an equivalent model) whose outer boundary was extended beyond the Alfvénic and sonic points. As a result, the overall structure of the solution has been imprinted by the MHD codes inner boundary condition. Therefore, different heliospheric MHD codes return the same general solution assuming they use the same magnetogram source to feed the WSA component. The heliospheric MHD codes do allow features in the solar wind imposed on their inner boundary to steepen and sharpen and can represent the development of shear-driven fluctuations. The WSA model, with its kinematic propagation approximation, cannot do this. However, in all validation work to date, the WSA model has used angular resolution of 1° or coarser. At these resolutions the fluctuations at the inner boundary of the MHD code do not sharpen to sufficiently small scales in transit to L1, which we would expect the MHD model RMSE to differ much from that of WSA. The WSA performance, for which there is a more extensive and coherent set of validation studies, therefore serves as a useful guide to, and comparative baseline for, the MHD model performance.

MacNeice (2009) analyzed the WSA model's performance in reproducing SIR arrival and IMF sector boundary crossings for the period from 1976 to 2008 and found WSA (with current sheet outer boundary located at 5

solar radii) to be worse than persistence for 1-day forecasts but better than persistence for longer forecast windows regardless of magnetogram source. They found that the model reported fewer HSEs (proxy for SIR arrival) than were observed, with a HSE hit rate of 40% and a false positive rate of 39%. They found that the IMF polarity was correctly reproduced approximately 80% of the time, a polarity reversal hit rate of about 60%, and a false positive rate of 11%. They found that the WSA performance was slightly degraded when the outer boundary of the current sheet component was located at 21.5 solar radii as is typical when supporting MHD model application in the heliosphere. These results support the conclusion that the WSA model is better at reproducing the magnetic topology than the details of the wind speed. These results were consistent with similar studies performed by Owens et al. (2005) and Owens et al. (2008).

Given that the WSA model has been empirically tuned to best fit the observed wind solutions at L1, we anticipate that the MHD model of the heliosphere can, at best, match the performance of the WSA model. This is indeed what we find. Overall, the MHD models achieve similar performance to the WSA models. They do of course provide much more complete solutions including parameters which WSA does not reproduce.

Gressl et al. (2014) reported similar SIR arrival time errors for MHD model runs during the year 2007 close to solar cycle minimum. Norquist (2013) reported similar results for the WSA/ENLIL model for the years 2007 through 2011, as did Lee et al. (2009) for the declining phase of solar cycle 23 and Jian et al. (2011) for time windows in both 2007 and the declining phase of cycle 23, with greater solar activity. These studies consistently report the following conclusions:

At L1,

- all solar wind models produce the best simulation results for the solar wind speed parameter, with proton temperature poorly reproduced (often off by an order of magnitude);
- the interplanetary sector structure (as coded in the radial magnetic field strength) is well reproduced, but medium-scale features, particularly in the neighborhood of the HCS, are not so well reproduced;
- for all models, the distributions of modeled solar wind parameters significantly differ from the measured distribution;
- model runs from WSA/ENLIL tested with different synoptic magnetic maps show significant differences in predicted arrival time and amplitudes of solar wind structures (e.g., Riley et al., 2012); however, there is no clear trend as to which synoptic map gives the best simulation results;
- the solutions are sensitive to how polar fields are reconstructed in the synoptic magnetograms; and
- all models give too small total magnetic field strengths (typically by a factor of order 2 (Lepri et al., 2008; Linker et al., 2017; Stevens et al., 2012).

Are these general trends repeated in the few studies based on data recorded at locations other than L1? Shiota et al. (2014) compared the solution from SUSANOO-SW for an interval between 2007 and 2009 with observations at L1, along with data recorded by MEX/ASPERA3 at Mars and VEX/ASPERA4 plasma measurements at Venus. Their results suggest that the model performance at the locations of Mars and Venus is comparable to that which the model records at L1.

Jian et al. (2016) used data from Ulysses from 2007 when its orbit took it from an extreme southern latitude to extreme northern latitude. Their RMSE analyses of wind speed indicate that the models outperformed 2-day persistence, with overall performance consistent with studies focussed at L1.

The assessment studies we have cited find no significant systematic difference in solution quality between quiet and active times. It is important to recognize that CMEs can modify the ambient wind in their wake, and so care must be taken in analyzing the quality of ambient wind solutions during solar maximum. Three points should be remembered. First, well-constructed assessment studies allow for this by excluding those times. Second, WSA and MHD models, using WSA to set their coronal solution, are dependent on the WSA tuning, which has evolved over the years but which generally attempts to achieve the best fit over both solar maximum and minimum. Third, the WSA model has been tuned on data over less than four full solar cycles and so the current-preferred tuning may not work as well for future cycles.

3.4. Eclipse Forecasts and Energization of the Corona

Predictions provide a rigorous test of the capabilities of models. Over the last two decades the group at PSI has taken advantage of total solar eclipses to test their models by predicting the shape of the white-light corona several weeks in advance. Such predictions can be compared with photographs of the corona subsequently taken during the eclipse (Mikić et al., 2007; Rusin et al., 2010) as illustrated in Figure 1.

July11, 2010 Total Solar Eclipse

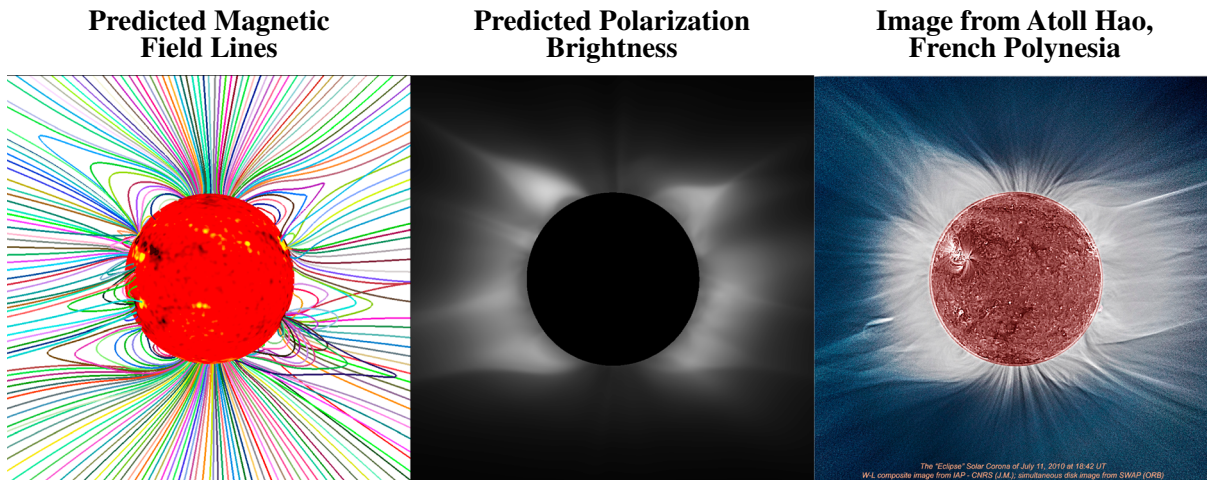| Predicted Magnetic Field Lines	Predicted Polarization Brightness	Image from Atoll Hao, French Polynesia

Figure 1. A comparison between a prediction of the corona, based on the MHD about a Sphere thermodynamic model, for the total solar eclipse of 11 July 2010 (left and center images), and an image of the eclipse (right) taken in French Polynesia (courtesy of Jean Mouette and Serge Koutchmy, Institut DAstrophysique de Paris, France). The images are oriented with solar north vertical.

Starting with a posteclipse simulation of the corona after the 3 November 1994 eclipse, 12 predictions have been performed, culminating with the recent eclipse on 21 August 2017 (Figure 2). In addition, the corona of the 20 March 2015 eclipse was studied after the fact. A recent investigation compares several models of the corona during this latest eclipse (Yeates et al., 2018).

This collection of PSI predictions is available at http://www.predsci.com/corona and provides a useful way to track the change in complexity of the solar corona as the Sun evolves between solar minimum and maximum. It also provides an instructive (if somewhat anecdotal) measure of the progress coronal models have made over the last two decades. As discussed in 2.4, starting with a polytropic MHD model of the 24 October 1995 eclipse, the PSI group eventually improved the description of the flow of energy in the corona by implementing a thermodynamic model with empirical coronal heating, including a transition region, radiative losses, and thermal conduction along the magnetic field lines (Lionello et al., 2001, 2009). The latest prediction of the 21 August 2017 eclipse used a wave-turbulence-driven heating model (Downs et al., 2016; Lionello, Velli, Downs, Linker, & Mikić, 2014; Lionello, Velli, Downs, Linker, Mikić, & Verdini, 2014; Verdini et al., 2010) in which the solar wind was accelerated and heated by Alfvén waves launched in the chromosphere (see 3.6).

The comparison of their results illustrates the extent to which these codes have evolved over the last 20 years and shows the level of physical complexity that they can accommodate when pushed to their limits.

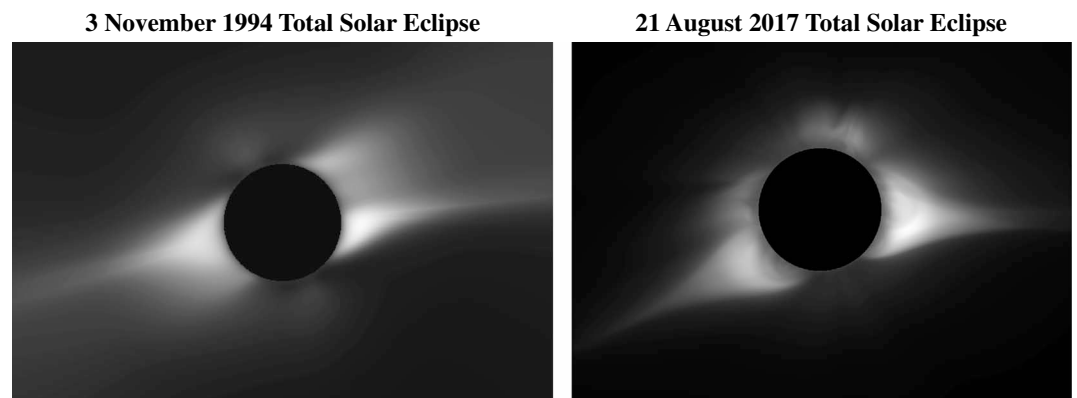| 3 November 1994 Total Solar Eclipse	21 August 2017 Total Solar Eclipse

Figure 2. Synthesized polarized brightness for the eclipses of 3 November 1994 and 21 August 2017 from the MHD about a Sphere model with thermodynamic energy equation and Alfvén wave heating.

The accuracy of the models has improved over time, as the underlying physical formulation was improved, and as computer power increased. The advent of massively parallel computers significantly improved the spatial resolution of the calculations. These improvements were driven, in large part, as a direct result of comparisons with eclipses. In addition to the white-light comparisons, the wealth of observations from SOHO/EIT and SDO/AIA in EUV wavelengths, and from Hinode/XRT in X-ray wavelengths, made it possible to improve the heating models, through comparisons of synthesized emission with observed emission.

For the latest 21 August 2017 prediction, the magnetic field was energized along filament channels, via emergence of transverse magnetic field, followed by flux cancellation to create flux ropes. This introduces magnetic shear along the polarity inversion lines that are typically the locations at which filaments (prominences) form (Mikić et al., 2018; Yeates et al., 2018). It produces an *inflated* appearance of streamers and pseudo-streamers in the lower corona that is typically inferred from eclipse images. The chirality of these flux ropes was determined by running a separate magnetofrictional model (Yeates, 2014) for the 7 months preceding the eclipse, fed by a surface flux transport model (Upton & Hathaway, 2014) that assimilated HMI magnetic field data. The locations of the flux ropes were determined by identifying filament channels in images and movies of SDO/AIA EUV emission. This process increased the free magnetic energy in the corona and led to a more realistic model of the magnetic field in the low corona (Mikić et al., 2018).

The energization of the corona has also been modeled by inserting flux ropes in selected active regions. This was done primarily for the purpose of initiating CMEs but is relevant for modeling the ambient corona during pre-eruption. PSI have used a modified Titov-Démoulin model (Titov et al., 2014, 2018). The group at the University of Michigan has a similar feature, called EEGGL, for CME modeling (e.g., Jin et al., 2017), but because they embed an unstable Gibson-Low flux tube, this cannot be used in its current form for ambient coronal modeling.

3.5. Advances in Understanding How to Drive Models Directly From Data

The promise of the high cadence and high-resolution vector magnetogram data from SDO/HMI led to the hope that these models could be driven directly by the observed temporal evolution of the photospheric field. Significant work has been done to understand how this might be done.

There are two main challenges in preparing the data to drive the MHD coronal field models. First, the data are incomplete for the purpose, and second, there are measurement errors in the data, which must be managed so they do not cause the MHD algorithms to fail. It is also the case that the inversion schemes used to produce the vector magnetogram data contain assumptions about the solar atmosphere that affect the resulting vector fields in subtle ways.

In principle, if we can derive the flow and magnetic field vectors on the surface, the time-evolving electric field can be computed at the model's lower boundary and this can be used to drive the MHD codes. In practice, because the data do not include vertical gradients of the field and flow vectors, it cannot completely define the field. Fisher et al. (2010), Fisher et al. (2012), and Kazachenko et al. (2014) have developed one method to address this issue. With the inclusion of additional data, such as that from Doppler LOS velocity measurements taken with HMI, and horizontal flows determined from local correlation tracking (e.g., Welsch et al., 2007), or other feature tracking approaches like DAVE4VM (Schuck, 2008), they have demonstrated that they can return an accurate solution in a test case for which the true electric field is known. This approach is applied in their Coronal Global Evolutionary Model suite (Fisher et al., 2015), which will be delivered to the CCMC shortly.

Whatever approach is used to define the surface information, it must then be incorporated into the field model in a manner that is consistent with the algorithm's design, its discretization approach, and its constraint equations. Obviously, codes that use nonspherical coordinates require additional spatial interpolation. To support this processing, MacNeice and Allred (2018) developed the MAGIC tools suite which is available for user download from the CCMC website.

It should be recognized that any observational data set inevitably includes measurement errors. Typically, the error bars associated with horizontal components of the magnetic field are larger than those associated with the LOS components. As a result, the observed surface fields are inconsistent with known physical constraints such as the solenoidal condition. The data must be modified to accommodate this before it can be safely applied within the models. It is not yet clear how best to achieve this. In addition, there is a known orbital phase signature in the HMI data that has yet to be fully understood (Schuck, Antiochos, et al., 2016; Schuck, Scherrer, et al., 2016). The correlation tracking programs require data with a cadence of 12 min or less for

stable reconstruction, given the HMI pixel sizes (Leake et al., 2017). Their results are therefore impacted by this problem, and until it is corrected, results of models driven directly by these data must be treated with caution.

To date, some attempts have been made with MHD and magnetofrictional codes driven by HMI data to model the evolution of active regions (e.g., Jiang et al., 2016; Hayashi et al., 2018; Yardley et al., 2018) but have not yet been applied to the global field.

3.6. Physically Motivated Heating, Turbulence, and Turbulent Energy

During their early development, almost all multidimensional models of the solar wind relied on simple volumetric heating formulae, not connected directly to any specific physical process. Typically, they also ignored the energy contained in subgrid-scale turbulence. Over the last half decade global MHD model developers have begun to include the influence of this subgrid-scale turbulence, and coronal and solar wind heating and acceleration sources based on specific physical processes. One example is heating and acceleration due to the dissipation of counter streaming Alfvén wave fluctuations (e.g., Chandran et al., 2011). The CORHEL (Downs et al., 2016), AWSoM_R (van der Holst et al., 2014), CRONOS (Wiengarten et al., 2016), and Usmanov et al. (2014) and Usmanov et al. (2018) models have all supplemented the basic MHD equations with a set of additional equations describing the energy content, transport, and dissipation of the Alfvén wave fluctuations. These codes have subtle differences. These include how their additional equations are derived, how they relate the energy in the subgrid-scale turbulence to shear in the shortest-scale fluctuations of their mean flow solution, their estimates of the energy dissipation rates feeding turbulent energy back into the plasmas internal energy, and the way the Alfvén wave energy fluxes are set at the inner boundary of the models. These modified codes do compare successfully with the general character of the observed corona and solar wind (Downs et al., 2016; Meng et al., 2015; Oran et al., 2017; Usmanov et al., 2018). While these developments represent a significant step toward a more complete self-consistent physical model, they are based on a description of the turbulence, which is greatly simplified. In particular, they make numerous assumptions about the form of the turbulence spectrum in the inertial range and impose phenomenological dissipation rates to specify the eventual transfer of energy from the turbulence to the plasmas internal energy. We anticipate that over the next decade, in situ observations made by the Parker Solar Probe and the Magnetospheric Multiscale Mission will test these turbulence treatments and their underlying assumptions.

3.7. Advances in Multifluid Algorithms

Heating by dissipation of counterstreaming Alfvén waves does not heat the electrons and ions equally. In addition, observations indicate that the ion distributions have different parallel and perpendicular temperatures. To accommodate both effects, the AWSoM (Oran et al., 2013) and Usmanov et al. (2014) models were developed with separate electron and proton temperatures. Oran et al. (2013) found that this gave a hotter and faster wind than in the equivalent single-temperature model heated by the same Poynting flux injected at the model base. This is principally because electron thermal conduction is more effective than proton thermal conduction. The finite thermal coupling between electrons and protons in the two temperature model slows the overall rate of cooling of the corona by conduction to the radiative sinks of the low corona and transition region.

AWSoM was extended by van der Holst et al. (2014) to allow also for distinct parallel proton and perpendicular proton temperatures, and its influence on the solar wind in the inner heliosphere was examined by Meng et al. (2015).

3.8. Enabling More Efficient Execution

Efficient execution becomes even more critical in enabling routine use of the most complex MHD models in a near-real-time operational environment. Improving time to solution is both a software and hardware challenge. Smarter AMR algorithms can focus computational effort where it is most effective. Porting algorithms to faster Graphics Processing Unit (GPU) chips can make best use of recent hardware developments.

3.8.1. Adaptive Mesh Techniques to Support Efficient High-Resolution Models

Adaptive Mesh Refinement allows models to focus the computational effort at points in the solution that require the most spatial resolution. For models of the ambient solar wind, this capability is most relevant in the lower coronal section of the combined model. As the MHD models of the coronal field evolve to include more detailed representations of fine structure within active regions and embedded flux ropes, AMR will be essential to achieve reasonable time to solution. A number of models already include the ability to adaptively refine the mesh or use fixed meshes that have higher resolution at preidentified locations. The Space Weather Modeling Framework was developed with a cartesian block adaptive foundation (Tóth et al.,

2012). Both the AMR Solar InterPlanetary space-time Conserving Element and Solution Element Solar Wind Model (Feng et al., 2012) and ENLIL (Odstrcil, 2003; Odstrcil et al., 2003) can use the PARAMESH AMR package (MacNeice et al., 2011). The CORHEL suite can use a fixed mesh with variable spacing, which concentrates mesh points at desired locations (e.g. Mok et al., 2016).

3.8.2. Porting Codes to GPUs

Inevitably, as physics-based models evolve to include additional physical processes and more complex field topologies and are required to execute in ensemble mode, they become more expensive to run. This poses a computational resource challenge to operational centers. Traditionally, this meant investing in large expensive computational systems or farming out model runs to remote supercomputers, which can lead to issues with accessibility, data transfer speeds, and guarantees of acceptable time to solution.

Recently, accelerated computing using GPU technology has become a viable alternative to traditional multi-core systems. GPUs can offer economical computation that is equivalent to hundreds or thousands of cores on traditional systems. They also allow facilities the planning flexibility to make small incremental increases to their computing power at low cost.

A number of developers of space weather models have already explored the use of GPUs (Germaschewski & Raeder, 2011). These early adopters needed major code rewrites to port their codes to the GPUs. The cost of developing a GPU version of their code while also maintaining and developing the existing code discouraged others from following this lead. Recent software developments have removed this impediment.

The OpenACC 2.0 standard (https://www.openacc.org) was established in 2013 (the current standard is OpenACC 2.6) and has opened the door for legacy codes to take advantage of GPU acceleration while maintaining compatibility with standard architectures. OpenACC allows the use of compiler directives that appear as comments in FORTRAN or C/C++ code. These directives identify portions of the code for acceleration, similar to the OpenMP standard. It offers a powerful set of constructs to accelerate computations on GPUs, while maintaining compatibility with existing MPI implementations.

The PSI group is now modifying the CORHEL suite to leverage these software developments (Caplan et al., 2017), and, if successful, would point the way for all other existing models to achieve similar performance boosts.

4. Model Inputs — Problems and Prospects

4.1. Magnetogram Issues

The ambient solar wind model solutions are determined, in large part, by the surface magnetic field information which sets the lower boundary conditions of the coronal field model. Almost all of the models of the ambient corona that have been used to drive solar wind models have used LOS magnetograms. There are a number of well-documented problems with these magnetograms.

1. Magnetograms from different observatories give fields with different amplitudes, amounting in some cases to factors as large as 4 (Riley et al., 2014).
2. Magnetograph measurements are computed assuming a spatially constant magnetic field and uniform atmosphere over a given detector pixel. In reality this assumption is never satisfied; the data are at best averages over unknown subresolution field structures, with response functions that vary depending on spectral and spatial resolution and integration time. Magnetogram calibration is dependent on polarimetric models to account for these spectral, spatial, and temporal resolution shortcomings. This can introduce significant differences to the *observed* flux levels (Leka & Barnes, 2012) and ultimately impact solar wind models.
3. Interpolation and rebinning when combining individual full disk magnetograms into synoptic maps can add further error, principally due to the temporal averaging of the time-varying field. Pevtsov et al. (2015) analyzed this by developing variance estimates (Bertello et al., 2014) for the NSO/SOLIS synoptic magnetograms and used them in ensemble mode to study their impact on the forecasts of the WSA/ENLIL model for L1. They estimated that the location of the HCS and photospheric neutral line could vary by as much as 5° in the PFSS solution and that error was propagated into the WSA/ENLIL wind solutions.
4. Polar fields are poorly measured. Because of the tilt of the Earth's orbit, the poles are alternately obscured producing data gaps. Also, the polar fields are mostly radial leading to low signal-to-noise ratio in LOS measurements. Both issues are usually managed using interpolation of fields from lower latitudes. Polar fields are critically important for determining the large-scale coronal magnetic field, as they affect the lower degree harmonics disproportionately.

5. Field measurements are only trusted from near disk center.
6. Most LOS instruments calculate radial fields by simply dividing the full-disk LOS field data by the cosine of the angle between the LOS and the solar surface normal. This procedure is generally accurate in weaker field regions where the true field is approximately radial, but it breaks down in sunspot active regions (Leka et al., 2017) and can cause serious errors in coronal field models, particularly in the topology of the HCS.
7. Global models require global surface fields provided through synoptic magnetograms. These synoptic magnetograms are constructed using measurements made within 60° longitude of disk center and used in global models under the assumption that the field does not change as the sun rotates. This is of course not true. Arge et al. (2013) have shown that active regions emerging on the far side modify the global solution enough to influence the solution on the near side.
8. Magnetograms are not uniformly sensitive to different levels of magnetic flux.

In addition, as shown by Toth et al. (2011), care must be taken when using potential field solvers based on spherical harmonic expansion, because of convergence issues associated with the near polar values of higher-order harmonics. For this reason they recommend using finite difference based solvers.

As we mentioned above in section 3.3, the models consistently underestimate the amount of open flux in the heliosphere. Given these issues with the magnetograms, that is hardly surprising.

Some of these deficiencies will be addressed through adoption of assimilative surface flux transport models of the solar field such as ADAPT, Surface Flux Transport (SURF), or Advective Flux Transport (AFT) (see section 4.2). Some may be addressed by adopting more complete vector magnetogram data sets. It should be noted that vector data has some issues of its own.

1. The LOS component of vector field data is significantly less noisy than the horizontal components.
2. Disambiguation of the vector field direction has to be imposed.
3. The most complete of these data sets, from SDO/HMI, has an orbital signature, which has yet to be properly characterized.

4.2. Surface Field Models
Many of the deficiencies of the synoptic magnetograms discussed in section 4.1 will be addressed through assimilative modeling of the evolving surface flux. Models such as ADAPT (Arge et al., 2010; Hickmann et al., 2015), SURF, AFT (Upton & Hathaway, 2014), and Evolving Surface Flux Transport Model (ESFTM) (Schrijver & De Rosa, 2003; e.g., Cameron et al., 2010) do this. ADAPT, for example, develops an ensemble of simulations of the time evolution of the surface flux using the Worden and Harvey model (Worden & Harvey, 2000), which includes the influence of differential rotation, meridional flow, supergranular diffusion, and random emergence of weak background flux. The Los Alamos National Laboratory Ensemble Kalman Filter data assimilation method is used to adjust the ADAPT model as new observational data becomes available. ADAPT maps are now routinely posted to the web, and coronal and solar wind models are beginning to use these as inputs (Linker et al., 2016, 2017; Merkin et al., 2016). The SURF model has been delivered to the CCMC and is being tested and configured for operation.

Preliminary testing of the models with ADAPT maps (Linker et al., 2016) does not yet show any marked improvement over results from the old static maps, but considerable recalibration and tuning of the WSA still needs to be done before comprehensive validation studies can be executed. When run in near real time, the leading polarity spots appear first in the ADAPT maps when an active region rotates around the east limb, and this can lead to an overall imbalance of positive and negative flux. Techniques to rebalance the flux are currently being investigated. In addition, these newly rotated east limb ARs may have appeared a few days earlier on the far side but can only be assimilated into the time-dependent map realizations once they are observed. This forced *catchup* can lead to errors in the global fields temporal evolution.

5. Research Topics Not Yet in Ambient Wind Models
5.1. Parameterization of Subscale Processes
Subscale physical processes affect the ambient wind solution in two ways. The first is through ubiquitous *volumetric* source terms in the MHD equations, which are really determined by kinetic processes. The obvious example would be the local heating and acceleration rates due to dissipation of fine-scale Alfvénic turbulence, which is discussed in sections 3.6 and 5.2. It would also include the rates of exchange of thermal energy and momentum between ions and electrons, which are known to have different temperatures and different

degrees of thermal anisotropy, resulting perhaps in the development of instabilities such as firehose and mirror (Kasper et al., 2006).

The second way is through the sensitivity of the large-scale solution to subscale processes at critical locations. The obvious example of this would be the way subscale processes set the true plasma resistivity and reconnection rates in the centers of current sheets. Classical estimates of the plasma resistivity in the corona and heliosphere are very low and so in practice in MHD codes this is always overwhelmed by numerical resistivity due to the finite resolution of the models. The true reconnection rates are determined by subgrid-scale kinetic physics. Particle codes and Hall-MHD codes are being used to study reconnection in these small-scale regimes. Although the physical reconnection process occurs at the small scales, there is both observational and modeling evidence to suggest that the effective large-scale reconnection rates are actually determined, through nonlinear small-scale evolution, by the macroscale conditions (Cassak et al., 2017). Studies are in progress to understand how to use these insights to control local resistivity in global MHD models, but it may be at least a decade before this is propagated forward into operational forecast models. These improvements will have a significant impact on MHD models of evolving coronal structure, on the nature of the HCS and the ability of the models to forecast B_z[1].

5.2. Time Dependence of the Solar Wind

The solar wind is unsteady, but its temporal evolution is still not well understood. It is instructive to consider the wind time dependence as a function of spatial scales in order to appreciate which aspects of the wind's time dependence may be better addressed by the MHD models in the near future.

At larger spatial scales ($> 10^5$ km) the ambient fast wind is relatively steady and the disturbances that do exist are small amplitude. At the finest scales ($< 10^2$ km) Alfvénic turbulence is observed, primarily propagating outward, and is believed to contribute to both heating and accelerating the wind. Between these scales, in what is known as the inertial range, the nonlinearity of the MHD equations causes some of the energy in the larger-scale disturbances to cascade to finer scales as the disturbances propagate outward. If and when this energy reaches the ion spatial scale it can be dissipated (e.g., Kiyani et al., 2015). A key question is, at a given point in the wind, how much of the local Alfvén wave flux is the result of injection and propagation from the Sun and how much is due to coarser disturbances near the Sun cascading to finer scales in transit from the Sun? Observations do not currently answer this question.

For MHD models of the fast wind in the ambient heliosphere, given current computational limitations, only the coarsest section of the inertial range is likely to be resolved in the next decade. Nevertheless, together with in situ observations from the Parker Solar Probe, successfully reproducing this section of the inertial range spectrum would determine the correct statistical description of coarser disturbances affecting the fast wind. It would then enable modelers to understand the role of specific processes such as the Kelvin-Helmholtz instability in the cascade. At the finest scales, more accurate characterization of the amplitude of fine-scale turbulence will define how the boundary fluxes and source terms for the Alfvén wave heating equations (see section 3.6) should be set.

In contrast to the fast wind, the slow wind is unsteady with large-amplitude fluctuations at all scales. The source of the slow wind is controversial. While everything we noted about the fast wind also applies to the slow wind, in addition the slow wind's large-amplitude fluctuations at the coarsest scale require that we understand the coronal structures that drive these. The slow solar wind is typically found surrounding the HCS and appears to have abundances similar to that of the closed corona. It appears to originate from a number of different coronal features (e.g., Cranmer et al., 2017).

A significant component of the slow wind clearly comes from larger structures formed by the boundaries of coronal holes and the outermost field lines of the streamers formed by the neighboring regions of closed field. Helmet streamers are not in equilibrium and their outermost closed field lines undergo periods of expansion and pinch-off through magnetic reconnection, releasing *blobs* of coronal plasma into the wind. These blobs are released intermittently at intervals ranging from hours for smaller blobs to tens of hours for larger ones (e.g., Viall & Vourlidas, 2015). The open field lines adjacent to pseudo-streamers have more complex topologies but are also believed to contribute to the slow wind.

---

[1] B_z is essentially the same as the RTN coordinate component B_N.

In the photosphere all open field lines are close to closed loops that comprise the magnetic carpet and it has been suggested that some of the slow wind is transferred from the closed carpet field lines to the open field lines through a constant process of local magnetic reconnection (e.g., Cranmer, 2018). Finally, the S-web concept can encompass all of these ideas. It postulates that the slow wind originates from a network of narrow open-field corridors which map to a web of separatrices and quasi-separatrix layers in the heliosphere (Antiochos et al., 2011).

SIRs represent the boundary between the fast and slow wind, and when the Sun is active, up to 50% of SIRs can be transient, indicating they vary much within one solar rotation (Jian et al., 2006).

Improving models of the coarse-scale slow wind structure will require using time-dependent high-resolution models of the corona driven by high cadence vector magnetograms (see sections 3.5 and 4.2). At present modeling of these slow wind source region theories is still restricted to idealized scenarios, and techniques to drive MHD codes using time-varying photospheric vector fields are still in the earliest stages of their development. We anticipate that it will take a decade before models of the streamer related and S-web sources will be mature enough, and computational platforms sufficiently powerful to support routine use in MHD forecasting models. The inclusion of slow wind sources associated with interchange reconnection between open field and closed magnetic carpet field lines may require significantly more resolution and would likely only be included in the next decade through some form of statistical parameterization.

5.3. Tomography Data

The physics behind the UCSD kinematic tomographic modeling becomes inadequate when used near the Sun, in regions very distant from it, or when exploring shock processes. To eliminate this deficiency in the kinematic tomography the UCSD group has produced a tomographic analysis whereby the IPS analysis can iteratively update 3-D MHD models as a kernel in the IPS time-dependent tomography. Used with both ENLIL and the Multi-Scale Flux Kinetic Simulation Suite 3-D MHD modeling to date this process allows an iterative best fit of 3-D MHD models to IPS data rather than the provision of 3-D MHD forward modeling from a lower boundary.

The ENLIL hybrid process UCSD has developed begins by providing the 3-D MHD model with a kinematic model boundary. The IPS-driven ENLIL model then outputs a first iteration volumetric matrix. The 3-D velocities and densities from this matrix are traced back to the source surface boundary and used with repeated boundary updates to the ENLIL model for an iterated solution best fit of the IPS data for velocity and density. By beginning a source surface with the kinematic modeling, inputs tests show that only three iterations are sufficient for a low resolution iterative ENLIL model convergence; this takes less than 6 hr of time on modest eight-node processors. While this technique provides better defined shock fronts, and nonradial plasma transport, this analysis has yet to be operated in real time (Jackson et al., 2018).

Future versions of this analysis are expected to use current 3-D MHD initiation techniques, such as ENLIL with current cone model technology or even more sophisticated 3-D MHD models that begin near the solar surface. In this way these models can be iteratively corrected for values of density, velocity, and magnetic fields as heliospheric structures move outward from the Sun. Weighted preference can be given for those parameters and timing values that are the best known and resolved both near the surface and remotely.

Current IPS tomographic technology is low resolution, with possibilities of at most a few thousand LOSs to scintillating radio sources per day, and the IPS analysis has ambiguities about the relationship between the proxy parameters for small-scale density variations observed and bulk density. This is not the same for heliospheric imagers that view Thomson scattering from heliospheric electrons (Jackson et al., 2004), and since the middle of the first decade of this century the CCMC has also hosted the Solar Mass Ejection Imager (SMEI) tomographic analysis at Runs on Request. Heliospheric imagers provide LOS measurements of as many as several hundreds of thousand per day, and tomographic resolutions in 3-D potentially commensurate with the cube root of these numbers. Updates of similar tomographic systems to SMEI are currently planned that include a NASA Small Explorer Mission scientific mission now in Phase A, the Polarimeter to Unify the Corona and Heliosphere (PUNCH), and a recently funded NASA operational mission concept, the All-Sky Heliospheric Imager. Both missions promote the extant SMEI tomographic system and updates to this system including a 3-D MHD analysis kernel for use in their proposed concept studies.

6. Conclusions

In this review we have assessed two types of models. The first type aims to use analytical/empirical relations, with the help of statistics and optimization to obtain the best prediction for the solar wind at the L1 point. The second type, the MHD models, use first-principle, physics-based forward modeling.

From an operational forecast perspective, for the limited set of parameters which they report (excepting B_z), empirical models such as AnEn, PROJECTZED, and PDF currently outperform semiempirical models like WSA which in turn matches or beats the MHD models. The limited validation data for the IPS based tomographic model HelTomo suggest that it achieves performance between that of the empirical and WSA model. The MHD models reproduce the interplanetary magnetic sector structure reasonably well, but all MHD models underestimate the global open flux by about a factor of 2. For wind properties at L1, the wind speed is the most reliable forecast followed by that of particle number density. Both plasma temperature and B_z are very poorly reproduced.

One might ask, *why do we need the expensive MHD models at all if the cheaper empirical models predict the solar wind to the same level or better?* The answer is, of course, that the cheaper models provide only partial information about the solar wind, while the MHD models offer insight into the underlying physics which we are trying to understand.

The pattern matching models beat all others in part because they use the L1 observations directly, while both WSA and MHD models use photospheric magnetogram data with significantly greater errors associated with both measurement and interpretation. Of course the empirical models do not support forecasting at locations other than L1 and offer relatively little scientific insight.

While not the focus of the present study, the pattern matching approaches also provide little scope for forecasting transient solar wind structures prior to their arrival at L1. In principle, once the leading edge of a transient structure has passed L1, pattern matching could provide a short-lead-time (< 24 hr) forecast of remaining structure (e.g., Chen et al., 1997), providing the historic solar wind record contains enough suitable analogues.

We anticipate that the near-real-time forecasts for both WSA and the MHD models will improve to match that of the empirical models, through the use of two approaches to intelligent preconditioning. With the use of ADAPT maps, an ensemble of at least 12 WSA-related models evolutions will be available. By comparing the WSA ADAPT forecasts to those of the empirical models, it should be possible to identify the best choice for the immediate forecast window and then submit these to the more computationally expensive MHD models. In addition, the preconditioning of the MHD solutions using the IPS tomography models will force the solution toward the observed wind state. Both of these preconditioning approaches are currently in development and should close the gap in forecast quality between the empirical and physics-based models. These developments will not improve the L1 forecast beyond that of the empirical models, but it should improve the model solution at other points in the heliosphere.

The MHD models have made great advances in recent years in supporting scientific research. More complete descriptions of the important physical process have been added, advances have been made in understanding how to craft and process time-dependent photospheric magnetic field maps, and the coronal field models have demonstrated the ability to model increasingly complex field topologies. The success of the July 2017 eclipse forecast in reproducing the observed complex coronal topology illustrates this. These new capabilities are still limited to scientific studies, but most can be expected to migrate into operational codes during the next decade.

The ability to accommodate more complex field topologies in the coronal MHD models, together with the use of high cadence and high resolution photospheric magnetic vector field observations to drive the models, offers the prospect, for the first time, of realistically representing the time dependence of the coarser-scale features in the ambient wind. An obvious example would be the larger plasma blobs released aperiodically from the tips of helmet streamers. Progress in representing finer scales will require improvements in the resolution and cadence of the observations used to drive the models.

We anticipate that in situ observations of the turbulence spectrum, including new near-Sun data from the Parker Solar Probe, will better inform how wave dissipation and other mechanisms are tuned to define local heating and acceleration.

The ever increasing sophistication and physical realism of the models will support a wealth of new scientific insights. However, this will not necessarily translate into improved operational forecast quality. An obvious question to pose is *when will the physics-based models outperform the empirical models?*. The case can be made that advances in model design have positioned the models to achieve this over the next decade. However, the pace of their development has outstripped the pace of improvements in the quality of the input data, which they consume, and until this is remedied, these models will not achieve their full forecasting potential.

References

Altschuler, M. D., & Newkirk, G. (1969). Magnetic fields and the structure of the solar corona. I: Methods of calculating coronal fields. *Solar Physics*, *9*, 131–149. https://doi.org/10.1007/BF00145734

Aly, J. J. (1989). On the reconstruction of the nonlinear force-free coronal magnetic field from boundary data. *Solar Physics*, *120*, 19–48. https://doi.org/10.1007/BF00148533

Amari, T., Aly, J. J., Luciani, J. F., Boulmezaoud, T. Z., & Mikić, Z. (1997). Reconstructing the solar coronal magnetic field as a force free magnetic field. *Solar Physics*, *174*, 129–149. https://doi.org/10.1023/A:1004966830232

Antiochos, S. K., Mikić, Z., Titov, V. S., Lionello, R., & Linker, J. A. (2011). A model for the sources of the slow solar wind. *The Astrophysical Journal*, *731*, 112. https://doi.org/10.1088/0004-637X/731/2/112

Arge, C. N., Henney, C. J., Gonzalez Hernandez, I., Toussaint, W. A., Koller, J., & Godinez, H. C. (2013). Modeling the corona and solar wind using ADAPT maps that include far-side observations. *AIP Conference Proceedings*, *1539*, 11–14. https://doi.org/10.1063/1.4810977

Arge, C. N., Henney, C. J., Koller, J., Compeau, C. R., Young, S., MacKenzie, D., et al. (2010). Air Force Data Assimilative Photospheric Flux Transport (ADAPT) model. *AIP Conference Proceedings*, *1216*, 343–346. https://doi.org/10.1063/1.3395870

Arge, C. N., & Pizzo, V. J. (2000). Improvement in the prediction of solar wind conditions using near-real time solar magnetic field updates. *Journal of Geophysical Research*, *105*(A5), 10,465–10,480. https://doi.org/10.1029/1999JA000262

Bertello, L., Pevtsov, A. A., Petrie, G. J. D., & Keys, D. (2014). Uncertainties in solar synoptic magnetic flux maps. *Solar Physics*, *289*, 2419–2431. https://doi.org/10.1007/s11207-014-0480-3

Bussy-Virat, C. D., & Ridley, A. J. (2014). Predictions of the solar wind speed by the probability distribution function model. *Space Weather*, *12*, 337–353. https://doi.org/10.1002/2014SW001051

Bussy-Virat, C. D., & Ridley, A. J. (2016). Twenty-four hour predictions of the solar wind speed peaks by the probability distribution function model. *Space Weather*, *14*, 861–873. https://doi.org/10.1002/2016SW001437

Cameron, R. H., Jiang, J., Schmitt, D., & Schussler, M. (2010). Surface flux transport modeling for solar cycles 15-21: Effects of cycle dependent tilt angles of sunspot groups. *The Astrophysical Journal*, *719*, 264–270. https://doi.org/10.1088/0004-637X/719/1/264

Caplan, R., Linker, J., & Mikić, Z. (2017). Presented at the NVIDIA GPU Technology Conference. http://on-demand.gputechconf.com/gtc/2017/video/s7535-ronald-caplan-potential-field-solutions-of-the-solar-corona-converting-a-pcg-solver-from-mpi-to-mpi+openacc.mp4.

Cassak, P. A., Liu, Y.-H., & Shay, M. A. (2017). A review of the 0.1 reconnection rate problem. *Journal of Plasma Physics*, *83*, 715830501. https://doi.org/10.1017/S0022377817000666

Chandran, B. D. G., Dennis, T. J., Quataert, E., & Bale, S. D. (2011). Incorporating kinetic physics into a two-fluid solar-wind model with temperature anisotropy and low-frequency Alfvén-wave turbulence. *The Astrophysical Journal*, *743*, 197. https://doi.org/10.1088/0004-637X/743/2/197

Chapman, S., & Bartels, J. (1940). *Geomagnetism*. London: Oxford University Press.

Chen, J., Cargill, P. J., & Palmadesso, P. J. (1997). Predicting solar wind structures and their geoeffectiveness. *Journal of Geophysical Research*, *102*(A7), 14,701–14,720. https://doi.org/10.1029/97JA00936

Chifu, I., Wiegelmann, T., & Inhester, B. (2017). Nonlinear force-free coronal magnetic stereoscopy. *The Astrophysical Journal*, *837*, 10. https://doi.org/10.3847/1538-4357/aa5b9a

Cohen, O. (2017). A comparison between physics-based and polytropic MHD models for stellar coronae and stellar winds of solar analogs. *The Astrophysical Journal*, *835*, 220. https://doi.org/10.3847/1538-4357/835/2/220

Cranmer, S. (2018). Low-frequency Alfvén waves produced by magnetic reconnection in the Sun's Magnetic Carpet. *The Astrophysical Journal*, *862*, 6. https://doi.org/10.3847/1538-4357/aac953

Cranmer, S. R., Gibson, S. E., & Riley, P. (2017). Origins of the ambient solar wind: Implications for space weather. *Space Science Reviews*, *212*, 1345–1384. https://doi.org/10.1007/s11214-017-0416-y

DeRosa, M. L., Schrijver, C. J., Barnes, G., Leka, K. D., Lites, B. W., Aschwanden, M. J., et al. (2009). A critical assessment of nonlinear force free field modeling of the solar corona for active region 10953. *The Astrophysical Journal*, *696*, 1780–1791. https://doi.org/10.1088/0004-637X/696/2/1780

DeRosa, M. L., Wheatland, M. S., Leka, K. D., Barnes, G., Amari, T., Canou, A., et al. (2015). The influence of spatial resolution on nonlinear force-free modeling. *The Astrophysical Journal*, *811*, 107. https://doi.org/10.1088/0004-637X/811/2/107

Den, M., Tanaka, T., Kubo, Y., & Watari, S. (2015). Three-dimensional MHD simulation of the solar wind from the solar surface to 400 solar radius using REPPU (REProduce Plasma Universe) code. In *Proceedings of the 34Th International Cosmic Ray Conference (ICRC2015). 30 July - 6 August 2015. The Hague, The Netherlands*.

Detman, T., Smith, Z., Dryer, M., Fry, C. D., Arge, C. N., & Pizzo, V. (2006). A hybrid heliospheric modeling system: Background solar wind. *Journal of Geophysical Research*, *111*, A07102. https://doi.org/10.1029/2005JA011430

Downs, C., Lionello, R., Mikić, Z., Linker, J. A., & Velli, M. (2016). Closed-field coronal heating driven by wave turbulence. *The Astrophysical Journal*, *832*, 180. https://doi.org/10.3847/0004-637X/832/2/180

Downs, C., Roussev, I. I., van der Holst, B., Lugaz, N., Sokolov, I. V., & Gombosi, T. I (2010). Toward a realistic thermodynamic magnetohydrodynamic model of the global solar corona. *The Astrophysical Journal*, *712*, 1219–1231. https://doi.org/10.1088/0004-637X/712/2/1219

Dunn, T., Jackson, B. V., Hick, P. P., Buffington, A., & Zhao, X. P. (2005). Comparative analyses of the CSSS calculation in the UCSD tomographic solar observations. *Solar Physics*, *227*, 339. https://doi.org/10.1007/s11207-005-2759-x

Echer, E., Korth, A., Bolzan, M. J. A., & Freidel, R. H. W. (2017). Global geomagnetic responses to the IMF b_z fluctuations during the September/October 2003 high speed stream intervals. *Annales Geophysicae*, *35*, 853–868. https://doi.org/10.5194/angeo-35-853-2017

Empirical Solar Wind Forecast (2018). http://swe.uni-graz.at/index.php/services/solar-wind-forecast.

Feng, X., Yang, L., Xiang, C., Jiang, C., Ma, X., Wu, S. T., et al. (2012). Validation of the 3D AMR SIP-CESE solar wind model for four Carrington rotations. *Solar Physics*, *279*, 207–229. https://doi.org/10.1007/s11207-012-9969-9

Fisher, G. H., Abbett, W. P., Bercik, D. J., Kazachenko, M. D., Lynch, B. J., Welsch, B. T., et al. (2015). The Coronal Global Evolutionary Model: Using HMI vector magnetogram and Doppler data to model the buildup of free magnetic energy in the solar corona. *Space Weather*, *13*, 369–373. https://doi.org/10.1002/2015SW001191

Fisher, G. H., Welsch, B. T., & Abbett, W. P. (2012). Can we determine electric fields and Poynting fluxes from vector magnetograms and doppler measurements? *Solar Physics*, *277*, 153–163. https://doi.org/10.1007/s11207-011-9816-4

Fisher, G. H., Welsch, B. T., Abbett, W. P., & Bercik, D. J. (2010). Estimating electric fields from vector magnetogram sequences. *The Astrophysical Journal*, *715*, 242–259. https://doi.org/10.1088/0004-637X/715/1/242

Fry, C. D., Sun, W., Deehr, C. S., Dryer, M., Smith, Z., Akasofu, S.-I., et al. (2001). Improvements to the HAF solar wind model for space weather predictions. *Journal of Geophysical Research*, *106*(A10), 20985–21002. https://doi.org/10.1029/2000JA000220

Gary, G. A. (2001). Plasma beta above a solar active region: Rethinking the paradigm. *Solar Physics*, *203*, 71–86. https://doi.org/10.1023/A:1012722021820

Gauss, C. F. (1839). Allgemeinetheorie des Erdmagnetismus. Resultate aus den Beobachtungen des magnetischen Vereins im Jahre 1838, 1.

Germaschewski, K., & Raeder, J. (2011). Using automated code generation to support high performance extended MHD integration in openGGCM. In *5th International Conference of Numerical Modeling of Space Plasma Flows*, pp. 197.

Gibson, S., Kucera, T., White, S., Dove, J., Fan, Y., Forland, B., et al. (2016). FORWARD: A toolset for multiwavelength coronal magnetometry. *Frontiers in Astronomy and Space Sciences*, *3*, 8. https://doi.org/10.3389/fspas.2016.00008

Gombosi, T. I., De Zeeuw, D. L., Groth, C. P., Powell, K. G., Clauer, C. R., & Song, P. (2001). From Sun to Earth: Multiscale MHD simulations of space weather. In P. Song, et al. (Eds.), *Space weather* (vol. 125, Geophysical Monograph Series. Washington, D. C.: AGU, pp. 169–176.

Gressl, C., Veronig, A. M., Temmer, M., Odstrcil, D., Linker, J. A., Mikić, Z., & Riley, P. (2014). Comparative study of MHD modeling of the background solar wind. *Solar Physics*, *289*, 1783–1801. https://doi.org/10.1007/s11207-013-0421-6

Hayashi, K. (2012). An MHD simulation model of time-dependent co-rotating solar wind. *Journal of Geophysical Research*, *117*, A08105. https://doi.org/10.1029/2011JA017490

Hayashi, K., Feng, X., Xiong, M., & Jiang, C. (2018). An MHD simulation of solar active region 11158 driven with a time-dependent electric field determined from HMI vector magnetic field measurement data. *The Astrophysical Journal*, *855*, 11. https://doi.org/10.3847/1538-4357/aaacd8

Hickmann, K. S., Godinez, H. C., Henney, C. J., & Arge, C. N. (2015). Data assimilation in the ADAPT photospheric flux transport model. *Solar Physics*, *290*(4), 1105–1118. https://doi.org/10.1007/s11207-015-0666-3

Jackson, B. V., Buffington, A., Hick, P. P., Altrock, R. C., Figueroa, S., Holladay, P. E., et al. (2004). The solar Mass-Ejection imager (SMEI) mission. *Solar Physics*, *225*, 177–207. https://doi.org/10.1007/s11207-004-2766-3

Jackson, B. V., Clover, J. M., Hick, P. P., Buffington, A., Bisi, M. M., & Tokumaru, M. (2013). Inclusion of real-time in-situ measurements into the UCSD time-dependent tomography and its use as a forecast algorithm. *Solar Physics*, *285*, 151–165. https://doi.org/10.1007/s11207-012-0102-x

Jackson, B. V., Hick, P. P., Bisi, M. M., Clover, J. M., & Buffington, A. (2010). Inclusion of in-situ velocity measurements into the UCSD time dependent tomography to constrain and better forecast remote sensing observations. *Solar Physics*, *265*, 245–256. https://doi.org/10.1007/s11207-010-9529-0

Jackson, B. V., Hick, P. P., & Buffington, A. (2002). Time-dependent tomography of heliospheric features using interplanetary scintillation (IPS) remote-sensing observations. In *Solar Wind 10 Conference Proceedings, Pisa, June 17–21*, pp. 31.

Jackson, B. V., Hick, P. P., Buffington, A., Bisi, M. M., Clover, J. M., Tokumaru, M., et al. (2011). Three-dimensional reconstruction of heliospheric structure using iterative tomography: A review. *Journal of Atmospheric and Solar-Terrestrial Physics*, *73*, 1214–1227. https://doi.org/10.1016/j.jastp.2010.10.007

Jackson, B. V., Hick, P. L., Kojima, M., & Yokobe, A. (1998). Heliospheric tomography using interplanetary scintillation observations 1. Combined Nagoya and Cambridge data. *Journal of Geophysical Research*, *103*(A6), 12049–12068. https://doi.org/10.1029/97JA02528

Jackson, B. V., Odstrcil, D., Yu, H.-S., Hick, P. P., Buffington, A., Mejia-Ambriz, J. C., et al. (2015). The UCSD kinematic IPS solar wind boundary and its use in the ENLIL 3D MHD prediction model. *Space Weather*, *13*, 104–115. https://doi.org/10.1002/2014SW001130

Jackson, B. V., Yu, H.-S., Buffington, A., Hick, P. P., Nishimura, N., Nozaki, N., et al. (2016). Exploration of solar photospheric magnetic field data sets using the tomography. *Space Weather*, *14*, 1107–1124. https://doi.org/10.1002/2016SW001481

Jackson, B. V., Yu, H.-S., Hick, P. P., Buffington, A., Odstrcil, D., Pogorelov, N., & Kim, T. (2018). Heliospheric tomography results using 3-D MHD kernels. Oral Presentation at the CCMC Workshop, 23-27 April, College Park, MD.

Jian, L. K., MacNeice, P. J., Mays, M. L., Taktakishvili, A., Odstrcil, D., Jackson, B., et al. (2016). Validation for global solar wind prediction using Ulysses comparison: Multiple coronal and heliospheric models installed at the Community Coordinated Modeling Center. *Space Weather*, *14*, 592–611. https://doi.org/10.1002/2016SW001435

Jian, L. K., MacNeice, P. J., Taktakishvili, A., Odstrcil, D., Jackson, B., Yu, H.-S., et al. (2015). Validation for solar wind prediction at Earth: Comparison of coronal and heliospheric models installed at the CCMC. *Space Weather*, *13*, 316–338. https://doi.org/10.1002/2015SW001174

Jian, L., Russell, C. T., Luhmann, J. G., MacNeice, P. J., Odstrcil, D., Riley, P., et al. (2011). Comparison of observations at ACE and ulysses with enlil model results: Stream interaction regions during carrington rotations 2016–2018. *Solar Physics*, *273*, 179–203. https://doi.org/10.1007/s11207-011-9858-7

Jian, L., Russell, C. T., Luhmann, J. G., & Skoug, R. M. (2006). Properties of stream interactions at one AU during 1995–2004. *Solar Physics*, *239*, 393–436. https://doi.org/10.1007/s11207-006-0133-2

Jiang, C., Wu, S. T., Feng, X., & Hu, Q. (2016). Data-driven magnetohydrodynamic modelling of a flux-emerging active region leading to solar eruption. *Nature Communications*, *7*, 11522. https://doi.org/10.1038/ncomms11522

Jin, M., Manchester, W. B., van der Holst, B., Sokolov, I., Toth, G., Mullinix, R. E., et al. (2017). Data-constrained Coronal Mass Ejections in a Global Magnetohydrodynamics Model. *The Astrophysical Journal*, *834*, 173. https://doi.org/10.1088/0004-637X/834/2/173

Kasper, J. C., Lazarus, A. J., Steinberg, J. T., Ogilvie, K. W., & Szabo, A. (2006). Physics-based tests to identify the accuracy of solar wind ion measurements: A case study with the Wind Faraday Cups. *Journal of Geophysical Research*, *111*, A03105. https://doi.org/10.1029/2005JA011442

Kazachenko, M. D., Fisher, G. H., & Welsch, B. T. (2014). A comprehensive method of estimating electric fields from vector magnetic field and Doppler measurements. *The Astrophysical Journal*, *795*, 17. https://doi.org/10.1088/0004-637X/795/1/17

Kiyani, K. H., Osman, K. T., & Chapman, S. C. (2015). Dissipation and heating in solar wind turbulence: From the macro to the micro and back again. *Philosophical Transactions of the Royal Society A*, *373*, 20140155. https://doi.org/10.1098/rsta.2014.0155

Leake, J. E., Linton, M. G., & Schuck, P. W. (2017). Testing the accuracy of data-driven MHD simulations of active region evolution. *The Astrophysical Journal*, *838*, 113. https://doi.org/10.3847/1538-4357/aa6578

Lee, C. O., Luhmann, J. G., Odstrcil, D., MacNeice, P. J., de Pater, I., Riley, P., & Arge, C. N. (2009). The solar wind at 1 AU during the declining phase of solar cycle 23: Comparison of 3D numerical model results with observations. *Solar Physics*, *254*, 155–183. https://doi.org/10.1007/s11207-008-9280-y

Leka, K. D., & Barnes, G. (2012). Modeling and interpreting the effects of spatial resolution on solar magnetic field maps. *Solar Physics*, *277*, 89. https://doi.org/10.1007/s11207-011-9821-7

Leka, K. D., Barnes, G., & Wagner, E. L. (2017). Evaluation (and Improving) estimates of the solar radial magnetic field component from line-of-sight magnetograms. *Solar Physics*, *292*, 36. https://doi.org/10.1007/s11207-017-1057-8

Lepri, S. T., Antiochos, S. K., Riley, P., Zhao, L., & Zurbuchen, T. H. (2008). Comparison of heliospheric in situ data with the quasi-steady solar wind models. *The Astrophysical Journal*, *674*, 1158–1166. https://doi.org/10.1086/524347

Levine, R. H., Schulz, M., & Frazier, E. N. (1982). Simulation of the magnetic structure of the inner heliosphere by means of a non-spherical source surface. *Solar Physics*, *77*, 363–392. https://doi.org/10.1007/BF00156118

Linker, J. A., Caplan, R. M., Downs, C., Lionello, R., Riley, P., Mikić, Z., et al. (2016). Downs an empirically driven time-dependent model of the solar wind. *Journal of Physics: Conference Series*, *719*, 12012. https://doi.org/10.1088/1742-6596/719/1/012012

Linker, J. A., Caplan, R. M., Downs, C., Riley, P., Mikić, Z., Lionello, R., et al. (2017). The open flux problem. *The Astrophysical Journal*, *848*, 70. https://doi.org/10.3847/1538-4357/aa8a70

Lionello, R., Linker, J. A., & Mikić, Z. (2001). Including the transition region in models of the large-scale solar corona. *The Astrophysical Journal*, *546*, 542–551. https://doi.org/10.1086/318254

Lionello, R., Linker, J. A., & Mikić, Z. (2003). Three dimensional magnetohydrodynamics of the solar corona and the solar wind with improved energy transport. *AIP Conference Proceedings*, *679*, 222–225. https://doi.org/10.1063/1.1618582

Lionello, R., Linker, & Mikić, Z. (2009). Multispectral emission of the sun during the first whole Sun month: Magnetohydrodynamic simulations. *The Astrophysical Journal*, *690*, 902–912. https://doi.org/10.1088/0004-637X/690/1/902

Lionello, R., Velli, M., Downs, C., Linker, J. A., & Mikić, Z. (2014). Application of a solar wind model driven by turbulence dissipation to a 2D magnetic field configuration. *The Astrophysical Journal*, *796*, 111. https://doi.org/10.1088/0004-637X/796/2/111

Lionello, R., Velli, M., Downs, C., Linker, J. A., Mikić, Z., & Verdini, A. (2014). Validating a time-dependent turbulence-driven model of the solar wind. *The Astrophysical Journal*, *784*, 120. https://doi.org/10.1088/0004-637X/784/2/120

Lionello, R., Velli, M., Linker, J. A., & Mikić, Z. (2013). Integrating physics-based coronal heating and solar wind acceleration in a global MHD model. *AIP Conference Proceedings*, *1539*, 30–33. https://doi.org/10.1063/1.4810982

Lockwood, M., Owens, M. J., Barnard, L. A., Bentley, S., Scott, C. J., & Watt, C. E. (2016). On the Origins and timescales of geoeffective IMF. *Space Weather*, *14*, 406–432. https://doi.org/10.1002/2016SW001375

Luhmann, J. G., Li, Y., Arge, C. N., Gazis, P. R., & Ulrich, R. (2002). Solar cycle changes in coronal holes and space weather cycles. *Journal of Geophysical Research*, *107*(A8), 1154. https://doi.org/10.1029/2001JA007550

MacNeice, P. J. (2009). Validation of community models: 2. Development of a baseline using the Wang-Sheeley-Arge model. *Space Weather*, *7*, S12002. https://doi.org/10.1029/2009SW000489

MacNeice, P., & Allred, J. (2018). MAGIC—MAGnetogram Interpolation and Composition. https://ccmc.gsfc.nasa.gov/support/MAGIC.

MacNeice, P., Olson, K. M., Mobarry, C., de Fainchtein, R., & Packer, C. (2011). PARAMESH V4.1: Parallel adaptive mesh refinement. Astrophysics Source Code Library, ascl:1106.009.

Mackay, D. H., & van Ballegooijen, A. A. (2006). Models of the large-scale corona. I. Formation, evolution, and liftoff of magnetic flux ropes. *The Astrophysical Journal*, *641*, 577–589. https://doi.org/10.1086/500425

Malanushenko, A., Schrijver, C. J., DeRosa, M. L., & Wheatland, M. S. (2014). Using coronal loops to reconstruct the magnetic field of an active region before and after a major flare. *The Astrophysical Journal*, *783*, 102. https://doi.org/10.1088/0004-637X/783/2/102

Malanushenko, A., Schrijver, C. J., DeRosa, M. L., Wheatland, M. S., & Gilchrist, S. A. (2012). Guiding nonlinear force-free modeling using coronal observations: First results using a quasi-Grad-Rubin scheme. *The Astrophysical Journal*, *756*, 153. https://doi.org/10.1088/0004-637X/756/2/153

Meng, X., van der Holst, B., Toth, G., & Gombosi, T. I. (2015). Alfvén wave solar model (AWSom): Proton temperature anisotropy and solar wind acceleration. *Monthly Notices of the Royal Astronomical Society*, *454*, 3697–3709. https://doi.org/10.1093/mnras/stv2249

Merkin, V. G., Lionello, R., Lyon, J. G., Linker, J., Török, T., & Downs, C. (2016). Coupling of coronal and heliospheric magnetohydrodynamic models: Solution comparisons and verification. *The Astrophysical Journal*, *831*, 23. https://doi.org/10.3847/0004-637X/831/1/23

Merkin, V. G., Lyon, J. G., McGregor, S. L., & Pahud, D. M. (2011). Disruption of a heliospheric current sheet fold. *Geophysical Research Letters*, *38*, L14107. https://doi.org/10.1029/2011GL047822

Metcalf, T. R., De Rosa, M. L., Schrijver, C. J., Barnes, G., van Ballegooijen, A. A., Wiegelmann, T., et al. (2008). Nonlinear force-free modeling of coronal magnetic fields. II. Modeling a filament arcade and simulated chromospheric and photospheric vector fields. *Solar Physics*, *247*, 269–299. https://doi.org/10.1007/s11207-007-9110-7

Mikić, Z., Downs, C., Linker, J. A., Caplan, R. M., Mackay, D. H., Upton, L. A., et al. (2018). *Predicting the corona for the 21 August 2017 total solar eclipse*. https://doi.org/10.1038/s41550-018-0562-5

Mikić, Z., Linker, J. A., Lionello, R., Riley, P., & Titov, V. (2007). Predicting the structure of the solar corona for the total solar eclipse of march 29, 2006. In O. Demircan, et al. (Eds.), *Solar and Stellar Physics Through Eclipses, ASP Conference Series Astronomical Society of the Pacific* (vol. 370, 299 pp.).

Mikić, Z, Linker, J. A., Schnack, D. D., Lionello, R., & Tarditi, A. (1999). Magnetohydrodynamic modeling of the global solar corona. *Physics of Plasmas*, *6*, 2217–2224. https://doi.org/10.1063/1.873474

Mok, Y., Mikić, Z., Lionello, R., Downs, C., & Linker, J. A. (2016). A three-dimensional model of active region: Comparison of simulations with observations. *The Astrophysical Journal*, *817*, 15. https://doi.org/10.3847/0004-637X/817/1/15

Nakamizo, A., Tanaka, T., Kubo, Y., Kamei, S., Shimazu, H., & Shinagawa, H. (2009). Development of the 3-D MHD model of the solar corona-solar wind combining system. *Journal of Geophysical Research*, *114*, A07109. https://doi.org/10.1029/2008JA013844

Norquist, D. C. (2013). Forecast performance assessment of a kinematic and a magnetohydrodynamic solar wind model. *Space Weather*, *11*, 17–33. https://doi.org/10.1029/2012SW000853

Norquist, D. C., & Meeks, W. C. (2010). A comparative verification of forecasts from two operational solar wind models. *Space Weather*, *8*, S12005. https://doi.org/10.1029/2010SW0005988

Odstrcil, D. (2003). Modeling 3-D solar wind structure. *Advances in Space Research*, *32*, 497–506. https://doi.org/10.1016/S0273-1177(03)00332-6

Odstrcil, D., Pizzo, V. J., Linker, J. A., Riley, P., Lionello, R., & Mikić, Z. (2004). Initial coupling of coronal and heliospheric numerical magnetohydrodynamic codes. *Journal of Atmospheric and Solar-Terrestrial Physics*, *66*, 1311–1320. https://doi.org/10.1016/j.jastp.2004.04.007

Odstrcil, D., Vandas, M., Pizzo, V. J., & MacNeice, P. (2003). Numerical simulation of interacting magnetic flux ropes. *AIP Conference Proceedings*, *679*, 699–702. https://doi.org/10.1063/1.1618690

Oran, R., Landi, E., van der Holst, B., Sokolov, I. V., & Gombosi, T. (2017). Alfvén wave turbulence as a coronal heating mechanism: Simultaneously predicting the heating rate and the wave-induced emission line broadening. *The Astrophysical Journal*, *845*, 98. https://doi.org/10.1088/0004-637X/845/2/98

Oran, R., van der Holst, B., Landi, E., Jin, M., Sokolov, I. V., & Gombosi, T. I. (2013). A global wave-driven magnetohydrodynamic solar model with a unified treatment of open and closed magnetic field topologies. *The Astrophysical Journal*, *778*, 176. https://doi.org/10.1088/0004-637X/778/2/176

Owens, M. J., Arge, C. N., Spence, H. E., & Pembroke, A. (2005). An event based approach to validating solar wind speed predictions: High speed enhancements in the Wang-Sheeley-Arge model. *Journal of Geophysical Research*, *110*, A12105. https://doi.org/10.1029/2005JA011343

Owens, M. J., Riley, P., & Horbury, T. S. (2017). Probabilistic solar wind and geomagnetic forecasting using an analogue ensemble or "similar day" approach. *Solar Physics*, *292*, 69. https://doi.org/10.1007/s11207-017-1090-7

Owens, M. J., Spence, H. E., McGregor, S., Hughes, W. J., Quinn, J. M., Arge, C. N., et al. (2008). Metrics for solar wind prediction models: Comparison of empirical, hybrid, and physics-based schemes with 8 years of L1 observations. *Space Weather*, *6*, S08001. https://doi.org/10.1029/2007SW000380

Peter, H., Warnecke, J., Chitta, L. P., & Cameron, R. H. (2015). Limitations of force-free magnetic field extrapolations: Revisiting basic assumptions. *Astronomy & Astrophysics*, *584*, A68. https://doi.org/10.1051/0004-6361/201527057

Pevtsov, A. A., Bertello, L., & MacNeice, P. (2015). Effect of uncertainties in solar synoptic magnetic flux maps in modeling of solar wind. *Advances in Space Research*, *56*, 2719–2726. https://doi.org/10.1016/j.asr.2015.05.043

Pizzo, V., Millward, G., Parsons, A., Biesecker, D., Hill, S., & Odstrcil, D. (2011). Wang-Sheeley-Arge-Enlil Cone model transitions to operations. *Space Weather*, *9*, S03004. https://doi.org/10.1029/2011SW000663

Pomoell, J., & Poedts, S. (2018). EUHFORIA: EURopean Heliospheric FORecasting Information Asset. *Journal of Space Weather and Space Climate*, *8*, A35. https://doi.org/10.1051/swsc/2018020

Powell, K. G., Roe, P. L., Linde, T. J., Gombosi, T. I., & De Zeeuw, D. L. (1999). A solution adaptive upwind scheme for ideal magnetohydrodynamics. *Journal of Computational Physics*, *154*(2), 284–309. https://doi.org/10.1006/jcph.1999.6299

Regnier, S., & Fleck, B. (2004). Proceedings of the SOHO 15 Workshop—Coronal Heating 6–9 September 2004. St. Andrews, Scotland, UK (ESA SP-575). Editors: R.W. Walsh, J. Ireland, D. Danesy, B. Fleck. Paris: European Space Agency, p.519.

Reiss, M. A., Temmer, M., Veronig, A. M., Nikolic, L., Vennerstrom, S., Schongassner, F., & Hofmeister, S. J. (2016). Verification of high-speed solar wind stream forecasts using operational solar wind models. *Space Weather*, *14*, 495–510. https://doi.org/10.1002/2016SW001390

Riley, P., Ben-Nun, M., Linker, J. A., Mikic, Z., Svalgaard, L., Harvey, J., et al. (2014). A multi-observatory intercomparison of line-of-sight synoptic solar magnetograms. *Solar Physics*, *289*, 769–792. https://doi.org/10.1007/s11207-013-0353-1

Riley, P., Ben-Nun, M., Linker, J. A., Owens, M. J., & Horbury, T. S. (2017). Forecasting the properties of the solar wind using simple pattern recognition. *Space Weather*, *15*, 526–540. https://doi.org/10.1002/2016SW001589

Riley, P., Linker, J. A., & Arge, C. N. (2015). On the role played by magnetic expansion factor in the prediction of solar wind speed. *Space Weather*, *13*, 154–169. https://doi.org/10.1002/2014SW001144

Riley, P., Linker, J. A., Lionello, R., & Mikić, Z. (2012). Corotating interaction regions during the recent solar minimum: The power and limitations of global MHD modeling. *Journal of Atmospheric and Solar-Terrestrial Physics*, *83*, 1–10. https://doi.org/10.1016/j.jastp.2011.12.013

Riley, P., Linker, J. A., & Mikić, Z. (2001). An empirically driven global MHD model of the solar corona and inner heliosphere. *Journal of Geophysical Research*, *106*(A8), 15,889–15,901. https://doi.org/10.1029/2000JA000121

Riley, P., Lionello, R., Linker, J. A., Mikić, Z., Luhmann, J., & Wijaya, J. (2011). Global MHD modeling of the solar corona and inner heliosphere for the whole heliospheric interval. *Solar Physics*, *274*, 361–377. https://doi.org/10.1007/s11207-010-9698-x

Roussev, I. I., Gombosi, T. I., Sokolov, I. V., Velli, M., Manchester, W., De Zeeuw, D. L., et al. (2003). A three dimensional model of the solar wind incorporating solar magnetogram observations. *The Astrophysical Journal Letters*, *595*, L57–L61. https://doi.org/10.1086/378878

Rusin, V., Druckmuller, M., Aniol, P., Minarovjech, M., Saniga, M., Mikić, Z., et al. (2010). Comparing eclipse observations of the 2008 August 1 solar corona with an MHD model prediction. *Astronomy and Astrophysics*, *513*, A45. https://doi.org/10.1051/0004-6361/200912778

Schatten, K. H. (1971). Current sheet magnetic model for the solar corona. *Cosmic Electrodynamics*, *2*, 232–245.

Schatten, K. H., Wilcox, J. M., & Ness, N. F. (1969). A model of interplanetary and coronal magnetic fields. *Solar Physics*, *6*, 442–455. https://doi.org/10.1007/BF00146478

Schrijver, C. J., & De Rosa, M. L. (2003). Photospheric and heliospheric magnetic fields. *Solar Physics*, *212*, 165–200. https://doi.org/10.1023/A:1022908504100

Schrijver, C. J., De Rosa, M. L., Metcalf, T. R., Liu, Y., McTiernan, J., Regnier, S., et al. (2006). Nonlinear force-free modeling of coronal magnetic fields part I: A quantitative comparison of methods. *Solar Physics*, *235*, 161–190. https://doi.org/10.1007/s11207-006-0068-7

Schrijver, C. J., DeRosa, M. L., Metcalf, T., Barnes, G., Lites, B., Tarbell, T., et al. (2008). Nonlinear force-free field modeling of a solar active region around the time of a major flare and coronal mass ejection. *The Astrophysical Journal*, *675*, 1637–1644. https://doi.org/10.1086/527413

Schuck, P. W. (2008). Tracking vector magnetograms with the magnetic induction equation. *The Astrophysical Journal*, *683*, 1134–1152. https://doi.org/10.1086/589434

Schuck, P. W., Antiochos, S. K., Leka, K. D., & Barnes, G. (2016). Achieving consistent Doppler measurements from SDO/HMI vector field inversions. *The Astrophysical Journal*, *823*, 101. https://doi.org/10.3847/0004-637X/823/2/101

Schuck, P. W., Scherrer, P., Antiochos, S. K., & Hoeksema, T. (2016). Achieving consistent vector magnetic field measurements from SDO/HMI. SDO 2016, Solar Dynamic Observatory, SDO-2016, SDO Workshop, SDO: 2016: Unraveling the Sun's Complexity.

Schulz, M., Frazier, E. N., & Boucher, D. J. (1978). Coronal magnetic field model with non-spherical source surface. *Solar Physics*, *60*, 83–104. https://doi.org/10.1007/BF00152334

Sheeley, N. R. Jr. (2017). Origin of the Wang-Sheeley-Arge solar wind model. *History of Geo- and Space Sciences*, *8*, 21–28. https://doi.org/10.5194/hgss-8-21-2017

Sheeley, N. R., & Wang, Y.-M. (1991). Magnetic field configurations associated with fast solar wind. *Solar Physics*, *131*, 165–186. https://doi.org/10.1007/BF00151752

Shiota, D., Kataoka, R., Miyoshi, Y., Hara, T., Tao, C., Masunaga, K., et al. (2014). Inner heliosphere MHD modeling system applicable to space weather forecasting for the other planets. *Space Weather*, *12*, 187–204. https://doi.org/10.1002/2013SW000989

Stevens, M. L., Linker, J. A., Riley, P., & Hughes, W. J. (2012). Underestimates of magnetic flux in coupled MHD model solar wind solutions. *Journal of Atmospheric and Solar-Terrestrial Physics*, *83*, 22–31. https://doi.org/10.1016/j.jastp.2012.02.005

Tadesse, T. (2015). Effect of the size of the computational domain on spherical nonlinear Force-Free modeling of a coronal magnetic field using SDO/HMI data. *Solar Physics*, *290*, 1159–1171. https://doi.org/10.1007/s11207-015-0664-5

Tadesse, T., Pevtsov, A. A., Wiegelmann, T., MacNeice, P. J., & Gosain, S. (2014). Global solar free magnetic energy and electric current density distribution of Carrington rotation 2124. *Solar Physics*, *289*, 4031–4045. https://doi.org/10.1007/s11207-014-0581-z

Titov, V. S. (2007). Generalized squashing factors for covariant description of magnetic connectivity in the solar corona. *The Astrophysical Journal*, *660*, 863–873. https://doi.org/10.1086/512671

Titov, V. S., Downs, C., Mikić, Z., Torok, T., Linker, J. A., & Caplan, R. M. (2018). Regularized Biot-Savart laws for modeling magnetic flux ropes. *The Astrophysical Journal Letters*, *852*, L21. https://doi.org/10.3847/2041-8213/aaa3da

Titov, V. S., Torok, T., Mikić, Z., & Linker, J. A. (2014). A Method for embedding circular force-free flux ropes in potential magnetic fields. *The Astrophysical Journal*, *790*, 163. https://doi.org/10.1088/0004-637X/790/2/163

Tóth, G., Sokolov, I., Gombosi, T. I., Chesney, D. R., Clauer, C. R., De Zeeuw, D., et al. (2005). Space weather modeling framework: A new tool for the space science community. *Journal of Geophysical Research*, *110*, A12226. https://doi.org/10.1029/2005JA011126

Toth, G., van der Holst, B., & Huang, Z. (2011). Obtaining potential field solutions with spherical harmonics and finite differences. *The Astrophysical Journal*, *732*, 102. https://doi.org/10.1088/0004-637X/732/2/102

Tóth, G., van der Holst, B., Sokolov, I. V., De Zeeuw, D. L., Gombosi, T. I., Fang, F., et al. (2012). Adaptive numerical algorithms in space weather modeling. *Journal of Computational Physics*, *231*, 870–903. https://doi.org/10.1016/j.jcp.2011.02.006

Upton, L., & Hathaway, D. H. (2014). Effects of meridional flow variations on solar cycles 23 and 24. *The Astrophysical Journal*, *792*, 142. https://doi.org/10.1088/0004-637X/792/2/142

Usmanov, A. V. (1993). A global numerical 3-D MHD model of the solar wind. *Solar Physics*, *146*, 377–396. https://doi.org/10.1007/BF00662021

Usmanov, A. V., Goldstein, M., & Matthaeus, W. H. (2014). Three-fluid, three-dimensional magnetohydrodynamic solar wind model with eddy viscosity and turbulent resistivity. *The Astrophysical Journal*, *788*, 43. https://doi.org/10.1088/0004-637X/788/1/43

Usmanov, A. V., Matthaeus, W. H., Goldstein, M. L., & Chhiber, R. (2018). The steady global corona and solar wind: A three-dimensional MHD simulation with turbulence transport and heating. *The Astrophysical Journal*, *865*, 25. https://doi.org/10.3847/1538-4357/aad687

van der Holst, B., Sokolov, I. V., Meng, X., Jin, M., Manchester, W. B., Toth, G., & Gombosi, T. I. (2014). Alfvén Wave Solar Model (AWSom): Coronal heating. *The Astrophysical Journal*, *782*, 81. https://doi.org/10.1088/0004-637X/782/2/81

Verdini, A., Velli, M., Matthaeus, W. H., Oughton, S., & Dmitruk, P. (2010). A turbulence driven model for heating and acceleration of the fast wind in coronal holes. *The Astrophysical Journal Letters*, *708*, L116–L120. https://doi.org/10.1088/2041-8205/708/2/L116

Viall, N. M., & Vourlidas, A. (2015). Periodic density structures and the origin of the slow solar wind. *The Astrophysical Journal*, *807*, 176. https://doi.org/10.1088/0004-637X/807/2/176

Wang, Y.-M., & Sheeley, N. R. Jr. (1990). Solar wind speed and coronal flux-tube expansion. *The Astrophysical Journal*, *355*, 726–732. https://doi.org/10.1086/168805

Warren, H. P., Crump, N. A., Ugarte-Urra, I., Sun, X., Aschwanden, M. J., & Wiegelmann, T. (2018). Toward a quantitative comparison of magnetic field extrapolations and observed coronal loops. *The Astrophysical Journal*, *860*, 13. https://doi.org/10.3847/1538-4357/aac20b

Welsch, B. T., Abbett, W. P., DeRosa, M. L., Fisher, G. H., Georgoulis, M. K., Kusano, K., et al. (2007). Tests and comparisons of velocity-inversion techniques. *The Astrophysical Journal*, *670*, 1434–1452. https://doi.org/10.1086/522422

Wiegelmann, T. (2007). Computing nonlinear force-free coronal magnetic fields in spherical geometry. *Solar Physics*, *240*, 227–239. https://doi.org/10.1007/s11207-006-0266-3

Wiegelmann, T. (2008). Nonlinear force-free modeling of the solar coronal magnetic field. *Journal of Geophysical Research*, *113*, A03S02. https://doi.org/10.1029/2007JA012432

Wiegelmann, T., Lagg, A., Solanki, S. K., Inhester, B., & Woch, J. (2005). Comparing magnetic field extrapolations with measurements of magnetic loops. *Astronomy and Astrophysics*, *433*, 701–705. https://doi.org/10.1051/0004-6361:20042421

Wiegelmann, T., Petrie, G. J. D., & Riley, P. (2017). Coronal magnetic field models. *Space Science Reviews*, *210*, 249–274. https://doi.org/10.1007/s11214-015-0178-3

Wiegelmann, T., & Sakurai, T. (2012). Solar force-free magnetic fields. *Living Reviews in Solar Physics*, *9*, 5. https://doi.org/10.12942/lrsp-2012-5

Wiengarten, T., Kleimann, J., Fichtner, H., Cameron, R., Jiang, J., Kissmann, R., & Scherer, K. (2013). MHD simulation of the inner heliospheric magnetic field. *Journal of Geophysical Research: Space Physics*, *118*, 29–44. https://doi.org/10.1029/2012JA018089

Wiengarten, T., Oughton, S., Engelbrecht, N. E., Fichtner, H., Kleimann, J., & Scherer, K. (2016). A generalized two-component model of solar wind turbulence and ab initio diffusion mean-free paths and drift length-scales of cosmic rays. *The Astrophysical Journal*, *833*, 17. https://doi.org/10.3847/0004-637X/833/1/17

Winebarger, A. R., Lionello, R., Mok, Y., Linker, J. A., & Mikić, Z. (2014). Verification of coronal loop diagnostics using realistic three-dimensional hydrodynamic models. *The Astrophysical Journal*, *795*, 138. https://doi.org/10.1088/0004-637X/795/2/138

Worden, J., & Harvey, J. (2000). An evolving synoptic magnetic flux map and implications for the distribution of photospheric magnetic flux. *Solar Physics*, *195*, 247–268. https://doi.org/10.1023/A:1005272502885

Yang, W. H., Sturrock, P. A., & Antiochos, S. K. (1986). Force-free magnetic fields: The magneto-frictional method. *The Astrophysical Journal*, *309*, 383–391. https://doi.org/10.1086/164610

Yardley, S. L., MacKay, D. H., & Green, L. M. (2018). Simulating the coronal evolution of AR 11437 using SDO/HMI magnetograms. *The Astrophysical Journal*, *852*, 82. https://doi.org/10.3847/1538-4357/aa9f20

Yeates, A. R. (2014). Coronal magnetic field evolution from 1996 to 2012: Continuous non-potential simulations. *Solar Physics*, *289*, 631–648. https://doi.org/10.1007/s11207-013-0301-0

Yeates, A. R., Amari, T., Contopoulos, I., Feng, X., Mackay, D. H., Mikić, Z., et al. (2018). Global non-potential magnetic models of the solar corona during the march 2015 eclipse. *Space Science Reviews*, *214*, 99. https://doi.org/10.1007/s11214-018-0534-1

Yeates, A. R., Mackay, D. H., & van Ballegooijen, A. A. (2007). Modelling the global solar corona: Filament chirality observations and surface simulations. *Solar Physics*, *245*, 87–107. https://doi.org/10.1007/s11207-007-9013-7

Yeates, A. R., Mackay, D. H., & van Ballegooijen, A. A. (2008). Modelling the global solar corona II: Coronal evolution and filament chirality comparison. *Solar Physics*, *247*, 103–121. https://doi.org/10.1007/s11207-007-9097-0

Yu, H. S., Jackson, B. V., Hick, P. P., Buffington, A., Odstrcil, D., Wu, C.-C., et al. (2015). 3D reconstruction of Interplanetary Scintillation (IPS) remote-sensing data: Global solar wind boundaries for driving 3D-MHD models. *Solar Physics*, *290*, 2519–2538. https://doi.org/10.1007/s11207-015-0685-0

Zhao, X., & Hoeksema, J. (1994). A coronal magnetic field model with horizontal volume and sheet currents. *Solar Physics*, *151*, 91–105. https://doi.org/10.1007/BF00654084

Zhu, X., & Wiegelmann, T. (2018). On the extrapolation of magneto-hydro-static equilibria on the Sun. arXiv:1809.02168.